This is an unofficial adaptation of an article that appeared in an ACS publication. ACS has not endorsed the content of this adaptation or the context of its use

Title

Radiosynthesis and *in vivo* evaluation of four PET tracer candidates for imaging of melatonin receptors

Authors

Hussein Bdair[*,1,2,§], Thomas A. Singleton[1,§], Karen Ross[1], Dean Jolly[1], Min Su Kang[3], Arturo Aliaga[3], Marius Tuznik[1], Tanpreet Kaur[4], Saïd Yous[5], Jean-Paul Soucy[1,6], Gassan Massarweh[1], Peter J. H. Scott[4], Robert Koeppe[4], Gilberto Spadoni[7], Annalida Bedini[7], David A. Rudko[1,8], Gabriella Gobbi[2], Chawki Benkelfat[2], Pedro Rosa-Neto[1, 3], Allen F. Brooks[*,4,§§], Alexey Kostikov[*,1,3,9,§§].

Affiliations

1 – McGill University, McConnell Brain Imaging Centre, Department of Neurology and Neurosurgery, Montreal Neurological Institute, Montreal, Quebec H3A 2B4, Canada.

2 – McGill University, Department of Psychiatry, Irving Ludmer Psychiatry Research and Training Building, Montreal, Quebec H3A 1A1, Canada.

3 – Translational Neuroimaging Laboratory, McGill University Research Centre for Studies in Aging, Alzheimer's Disease Research Unit, Douglas Research Institute, Le Centre intégré universitaire de santé et de services sociaux (CIUSSS) de l'Ouest-de-l'Île-de-Montréal, Montreal, Quebec H4H 1R3, Canada.

4 – University of Michigan Medical School, Department of Radiology, Ann Arbor, Michigan 48109-5610, United States.

5 – University of Lille, Lille Neurosciences and Cognition Research Center, Lille, Hauts-de-France FR 59000, France

6 – Concordia University, PERFORM Centre, Montreal, Québec H4B 1R6, Canada

7 – University Carlo Bo, Department Biomolecular Science, Urbino IT 61029, Italy

8 – Department of Biomedical Engineering, McGill University, Montreal, Quebec H3A 2B4, Canada

9 – McGill University, Department of Chemistry, Montreal, Quebec H3A 0B8, Canada.

Corresponding Authors

*Email: hussein.bdair@mail.mcgill.ca; Phone: (514) 398-8595

*Email: alexey.kostikov@mcgill.ca; Phone: (514) 398-1503

*Email : afb@umich.edu; Phone: (734) 615-1869

Keywords

Melatonin, Agomelatine, Melatonin receptors, Positron Emission Tomography, PET, Carbon-11, Fluorine-18, [^{11}C]UCM765, [^{11}C]UCM1014, [^{18}F]3FAGM, [^{18}F]FAAGM.

Abstract

Melatonin is a neurohormone that modulates several physiological functions in mammals through the activation of melatonin receptors type 1 and 2 (MT_1 and MT_2). The melatonergic system is an emerging therapeutic target for new pharmacological interventions in the treatment of sleep and mood disorders, thus imaging tools to further investigate its role in the brain are highly sought-after. We aimed to develop selective radiotracers for *in vivo* imaging of both MT_1 and MT_2 by positron emission tomography (PET). We identified four previously reported MT ligands with picomolar affinities to the target based on different scaffolds which were also amenable for radiolabeling with either carbon-11 or fluorine-18. [^{11}C]UCM765, [^{11}C]UCM1014, [^{18}F]3-fluoroagomelatine ([^{18}F]3FAGM) and [^{18}F]fluoroacetamidoagomelatine ([^{18}F]FAAGM) have

been synthesized in high radiochemical purity and evaluated in wild-type rats. All four tracers showed moderate to high brain permeability in rats with maximum standardized uptake values (SUV_{max} of 2.53, 1.75, 3.25 and 4.47, respectively) achieved 1–2 minutes after tracer administration followed by a rapid washout from the brain. Several melatonin ligands failed to block the binding of any of the PET tracer candidates, while in some cases homologous blocking surprisingly resulted in increased brain retention. Two ^{18}F-labeled agomelatine derivatives were brought forward to PET scans in non-human primates and autoradiography on human brain tissues. No specific binding has been detected in blocking studies. To further investigate pharmacokinetic properties of the putative tracers, microsomal stability, plasma protein binding, logD and membrane bidirectional permeability assays have been conducted. Based on the results, we conclude that the fast first pass metabolism by the enzymes in liver microsomes is the likely reason of the failure of our PET tracer candidates. Nevertheless, we showed that PET imaging can serve as a valuable tool to investigate the brain permeability of new therapeutic compounds targeting the melatonergic system.

Introduction

Melatonin (*N*-acetyl-5-methoxytryptamine; MLT) is a sleep-inducing hormone secreted in the central nervous system (CNS) of mammals mainly from the pineal gland during the dark phase of the light/dark cycle.[1] MLT regulates circadian rhythms *via* activation of two types of G protein-coupled receptors (GPCR) of the $G_{i/o}$ type, known as melatonin type 1 and 2 (MT_1 and MT_2) receptors.[2] Each receptor is located in specific areas of the brain[3,4] and has a distinct function in the regulation of neurophysiological functions.[5] Besides their role in sleep, circadian rhythm and pain, a growing body of literature suggests that aberrant expression of melatonin receptors is implicated in the pathogenesis of neuropsychiatric disorders (anxiety and depression)[6] and

neurodegenerative diseases, including Alzheimer's disease (AD),[7,8] Parkinson's disease (PD)[9] and Huntington's disease (HD).[10] Therefore, the melatonergic system has recently emerged as a promising therapeutic target.[6,11,12] Synthetic MLT has been extensively used as an over-the-counter medication for the treatment of insomnia.[13] In the last two decades, several non-selective MT_1/MT_2 agonists with longer biological half-lives have been approved for the treatment of sleep disorders, including ramelteon, tasimelteon and agomelatine.[14] The latter is also approved in Europe as an atypical antidepressant for treatment of major depressive disorder,[15] and showed efficacy in depression associated with neurodegenerative diseases[16] and other co-morbid conditions.[17] Accordingly, there is an emerging demand for the development of ligands selective to distinct melatonin receptor types. Several reviews on MT_1 and MT_2 selective synthetic ligands have been recently published.[18,19]

Despite these fast pharmacological advances, neuroanatomical mapping of melatonin receptor distribution in mammalian brains remains incomplete, particularly due to the dearth of reliable specific antibodies[20] as well as MT_1 and MT_2 selective radioligands.[21] Autoradiography studies using 2-[^{125}I]iodomelatonin[22] (Figure 1) greatly contributed to the pharmacological characterization and localization of MT receptors in the 80's and 90's.[23,24] While the results were inconsistent, most publications reported expression of melatonin binding sites with B_{max} values in the range of 3 to 50 fmol/mg protein in small hypothalamic nuclei, including suprachiasmatic nucleus (SCN), median eminence (ME) and pars tuberalis in pituitary gland, and in cerebellar cortex across several mammalian species.[25–29] Although 2-[^{125}I]iodomelatonin binds to melatonin binding sites with low picomolar affinity (reported K_d's in the range of 10 to 80 pM),[25–29] it does not differentiate between MT_1 and MT_2 and it has been suggested that dimerization of melatonin receptors can significantly reduce the number of available binding sites.[30] Recently,

immunohistochemistry studies[3] and knock-in genetic strategy replacing MT_1 or MT_2 coding sequences with a LacZ reporter[4] have reported that MT_1 and MT_2 receptors are localized in distinct regions; for example, MT_2 were found mostly in the thalamic regions, hippocampus and brainstem. The Human Protein Atlas database reports basal ganglia (BG) as the only region of MT_2 localization in the human brain on the RNA level (MTNR1B gene), but on a protein level it is found in the cortex, hippocampus, caudate and cerebellum; yet in pigs the highest expression of MT_2 was found in the midbrain, pons/medulla and corpus callosum.[31] According to the same atlas, the MT_1-encoding gene MTNR1A is instead localized mostly in the human cerebellum, while in pigs it is localized primarily in the hypothalamus and pituitary gland.[32] The Allen Brain Atlas reports MT_2 in the mouse brain only in negligible amounts in the cerebellum and does not report any expression of MT_1.[33] In addition, neither autoradiographic nor immunohistochemistry methods allow for *in vivo* imaging of MT_1 and MT_2. Accordingly, there is a great necessity to develop imaging tools with high selectivity and specificity to MT receptors for the visualization of their localization, concentration and function in different brain regions in living organisms, as well as for the development of new drugs targeting the melatonergic system.

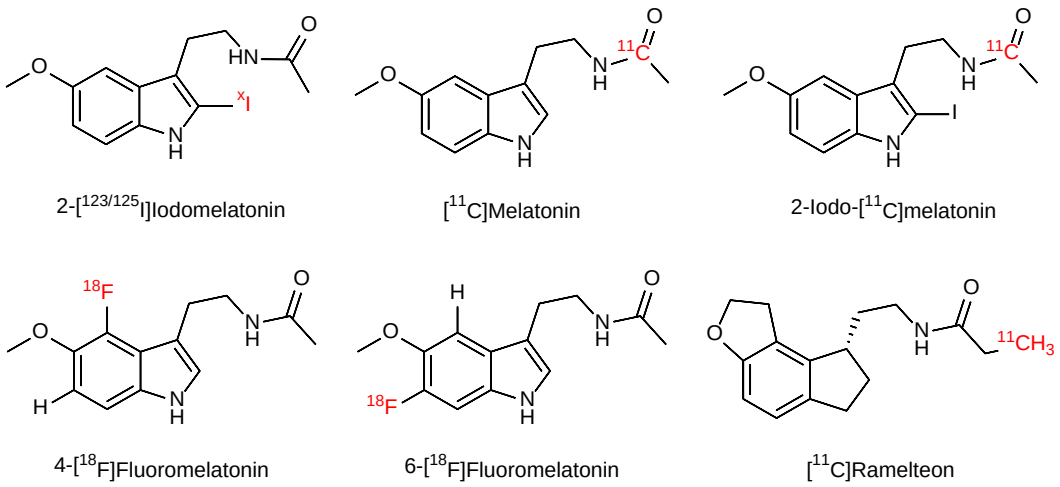

Figure 1. Previously developed melatonergic radiotracers.

Positron emission tomography (PET) is a powerful tool in neuroimaging studies for *in vivo* imaging of receptor expression. To date, none of the radioligands labelled with either carbon-11 or fluorine-18 have been validated as potential PET tracers for melatonin receptor imaging despite significant efforts in the early days of PET imaging developments (Figure 1). Thus, [^{11}C]MLT showed no specific binding in the brain despite fast permeation of the blood brain barrier,[34] most likely due to competition with endogenous MLT resulting in poor molar activity *in vivo*. PET imaging using either 4- or 6-[^{18}F]fluoromelatonin synthesized *via* electrophilic ^{18}F-fluorination of MLT has not been reported;[35] however, it can be assumed that at the obtained molar activities of below 0.01 GBq/µmol no specific binding would be observed. 2-Iodo-[^{11}C]melatonin was synthesized with a moderate molar activity of 11–22 GBq/µmol and advanced to imaging in human subjects, but no specific binding was detected as the tracer was rapidly cleared from the brain.[36] The isotopologue 2-[^{123}I]iodomelatonin was suggested as a SPECT tracer, but also did not reveal any specificity, presumably due to rapid *in vivo* deiodination.[37] Most recently, [^{11}C]ramelteon was labeled *via* ^{11}C-acylation in high decay-corrected radiochemical yield (RCY) and modest molar activity, but no biological evaluation of this PET tracer was reported.[38]

To the best of our knowledge, no attempt to evaluate MT-selective PET tracers was reported since the 1990's. Recent developments in pharmacology yielded numerous novel, more potent and selective MT ligands, while modern PET scanners offer significantly higher sensitivity and resolution compared to the technology used in earlier studies. These advances prompted us to reinvigorate the efforts to develop MT specific PET tracers. We identified four previously-reported ligands with K_i values below 100 pM to at least one of the MT receptor types and amenable for radiolabeling with one of the most common PET isotopes, carbon-11 or fluorine-18 (Figure 2). **UCM765**[39] is a selective MT_2 partial agonist which has been reported to promote non-rapid eye

movement sleep (NREMS) maintenance,[40] and has anxiolytic[41] and antinociceptive properties[42] in experimental animals. **UCM1014**[43] is a more recently developed full agonist with improved affinity towards MT_2 and a 17000-fold selectivity over MT_1. Both of these ligands contain methoxy groups, making them amenable for radiolabeling via ^{11}C-methylation for subsequent evaluation as MT_2-selective PET tracers. Two isomeric fluoroagomelatine derivatives, *N*-(2-(3-fluoro-7-methoxynaphthalen-1-yl)ethyl)acetamide (3-fluoroagomelatine) and 2-fluoro-*N*-(2-(7-methoxynaphthalen-1-yl)ethyl)acetamide (fluoroacetamidoagomelatine), respectively termed **3FAGM** and **FAAGM** hereafter, were reported as part of a structure-activity relationship study aiming to improve affinity and metabolic stability of the parent agomelatine.[44] Both compounds are among the most potent ligands, with nearly equipotent picomolar affinities to MT_1 and MT_2. Hence, their ^{18}F-fluorinated analogs could serve as PET tracers for non-selective imaging of MT receptors. Besides high affinities to the target, all four molecules displayed good to excellent calculated CNS multiparameter optimization (MPO) scores (Table 1). The CNS MPO score was developed by Wager *et al*.[45,46] as a predictive tool for brain permeability of drug candidates by assigning the score between 0 and 6.0 based on six physicochemical properties. CNS MPO has been widely adopted in PET tracer development for brain imaging with the score of 4.0 as a threshold to select the candidates with higher probability of brain entry. All four ligands satisfy this requirement. In this study, we report the radiosyntheses and *in vivo* studies of brain permeability, CNS regional distribution and washout rate for these four ligands in rats and non-human primates and their evaluation as PET tracer candidates for the imaging of melatonin receptors.

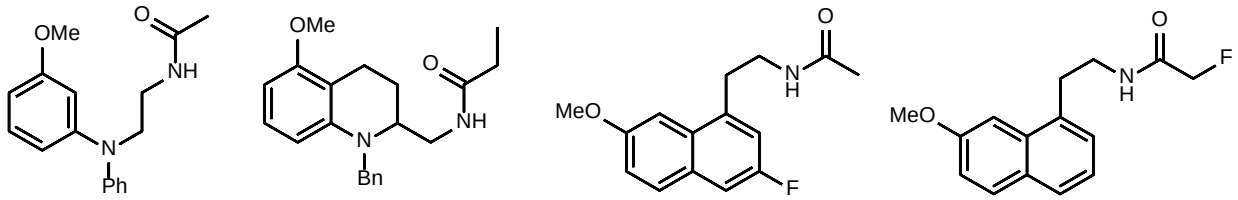

Figure 2. Structures of the reported MT ligands selected for radiolabeling with carbon-11 or fluorine-18.

Table 1. Affinities to MT_1/MT_2 and CNS MPO scores of the selected ligands.

Ligand	K_i MT_1, nM	K_i MT_2, nM	CNS MPO
UCM765[39]	4.2	0.066	5.58
UCM1014[43]	17	0.001	4.42
3FAGM[44]	0.1	0.07	5.66
FAAGM[44]	0.07	0.07	5.69

Results and discussion.

Chemistry. *N*-(2-((3-methoxyphenyl)(phenyl)amino)ethyl)acetamide (**UCM765**),[39] *N*-((1-benzyl-5-methoxy-1,2,3,4-tetrahydroquinolin-2-yl)methyl)propionamide (**UCM1014**),[43] *N*-(2-(3-fluoro-7-methoxynaphthalen-1-yl)ethyl)acetamide (3-fluoroagomelatine, **3FAGM**) and 2-fluoro-*N*-(2-(7-methoxynaphthalen-1-yl)ethyl)acetamide (fluoroacetamidoagomelatine, **FAAGM**)[44] have been synthesized according to the previously reported procedures and used as non-radioactive standards for the optimization of conditions for both preparative and analytical high performance liquid chromatography (HPLC). The former two compounds were treated with boron tribromide to yield desmethyl precursors **dmUCM765** and **dmUCM1014** for subsequent radiosyntheses of [^{11}C]UCM765 and [^{11}C]UCM1014, respectively, via ^{11}C-methylation. Boronic acid pinacolate precursor *N*-(2-(7-methoxy-3-(4,4,5,5-tetramethyl-1,3,2-dioxaborolan-2-yl)naphthalen-1-

yl)ethyl)acetamide (**3-BpinAGM**) for the radiosynthesis of [^{18}F]3FAGM was synthesized via Miyaura borylation from the previously reported *N*-(2-(3-bromo-7-methoxynaphthalen-1-yl)ethyl)acetamide (3-bromoagomelatine, **3-BrAGM**). 2-Bromo-*N*-(2-(7-methoxynaphthalen-1-yl)ethyl)acetamide (bromoacetamidoagomelatine, **BrAAGM**), the precursor for the radiosynthesis of [^{18}F]FAAGM, was synthesized by acylation of 2-(7-methoxynaphthalen-1-yl)ethan-1-amine with bromoacetyl bromide. Syntheses of all four precursors starting from either commercially available or previously reported compounds are summarized on Scheme 1.

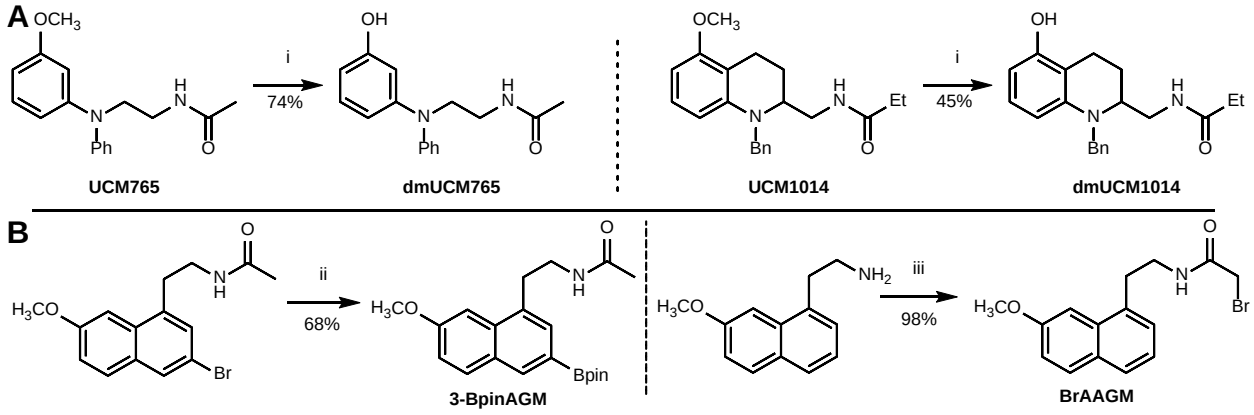

Scheme 1. A) Syntheses of desmethyl precursors for ^{11}C-labeled tracers based on UCM ligands; B) Syntheses of precursors for ^{18}F-labeled tracers based on agomelatine derivatives. i) BBr_3, DCM, 0 °C – r.t., 18 h; ii) B_2pin_2, $PdCl_2$(dppf), KOAc, DMSO, 80 °C, 18 h; iii) $BrCH_2COBr$, $CHCl_3$, r.t., 30 min.

Radiochemistry. [^{11}C]UCM765 and [^{11}C]UCM1014 were synthesized from the corresponding desmethyl precursors **dmUCM765** and **dmUCM1014** , respectively, and [^{11}C]CH_3I in DMSO in the presence of sodium hydroxide at 90 °C (Scheme 2). Both tracers were produced in moderate isolated decay-corrected radiochemical yields (RCY) of 17–22% (n = 4) and 18% (n = 1), respectively, with radiochemical purities (RCP) of >99% and molar activities (A_m) of 372 ± 60 GBq/μmol in 18–22 minutes.

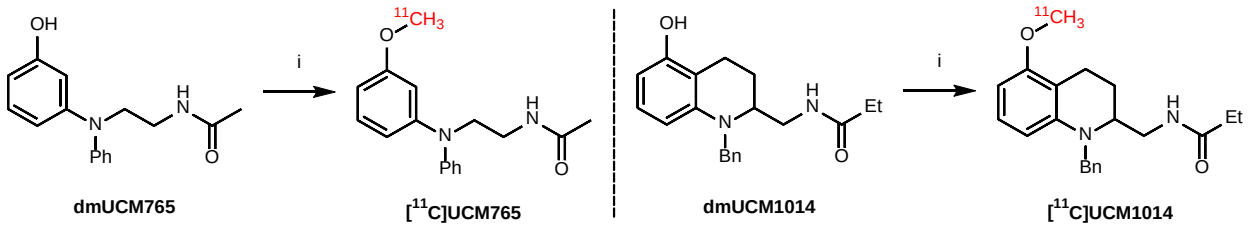

Scheme 2. Radiosynthesis of [^{11}C]UCM765 and [^{11}C]UCM1014 as PET tracer candidates for selective imaging of MT_2. i) [^{11}C]CH_3I, DMSO, 5 M NaOH, 90 °C, 5 min.

[^{18}F]3FAGM was synthesized via late-stage copper-catalyzed ^{18}F-fluorination of the corresponding boronic acid pinacolate precursor **3BpinAGM** in a 2:1 DMA/1-butanol mixture at 130 °C with a decay-corrected RCY of 20.3 ± 6.6 %, an RCP of >99 % and A_m of 108.7 ± 47.5 GBq/µmol in 75 minutes (n = 2) (Scheme 3, left). [^{18}F]FAAGM was synthesized via S_N2 substitution of the bromide in the corresponding bromoacetamide precursor **BrAAGM** at 100 °C in acetonitrile for 15 minutes with a decay-corrected RCY of 10.7 ± 6.6 %, an RCP of >99 % and A_m of 281.9 ± 147.5 GBq/µmol in 55 minutes (n = 2) (Scheme 3, right).

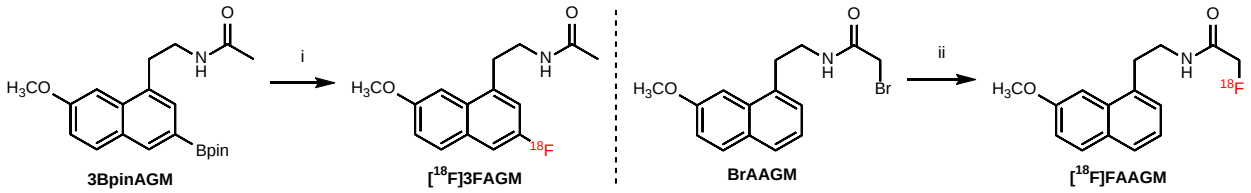

Scheme 3. Radiosynthesis of [^{18}F]3FAGM and [^{18}F]FAAGM as PET tracer candidates for imaging of MT_1 and MT_2. i) [^{18}F]Et_4NF, $Cu(OTf)_2py_4$, DMA/1-BuOH, 130 °C, 20 min; ii) [^{18}F]KF, K_2CO_3/K_{222}, MeCN, 100 °C, 15 min.

All tracers were purified by preparative HPLC and reformulated in dilute ethanol solution in saline suitable for intravenous injection in animals. Radiochemical and chemical purities, ligand

identities and molar activities were determined by analytical HPLC prior to tracer injection into animals.

PET imaging in rodents. [^{11}C]UCM765 and [^{11}C]UCM1014 were evaluated first as PET tracer candidates for selective imaging of MT_2 receptor in wild-type Sprague Dawley rats to determine their brain permeation, regional distribution and clearance rate. Baseline [^{11}C]UCM765 scans revealed that the tracer rapidly crosses the BBB, with a whole brain SUV_{max} of 2.53 ± 0.45 (n = 4) achieved 30 s post injection (Figure 3). The tracer shows nearly homogenous distribution in all analyzed brain regions despite the minor differences in the initial uptake in the following order: thalamus (SUV_{max} = 3.00 ± 0.42), hippocampus (SUV_{max} = 2.62 ± 0.40), cerebellum (SUV_{max} = 2.53 ± 0.50), hypothalamus (SUV_{max} = 2.51 ± 0.49) and cortex (SUV_{max} = 2.34 ± 0.49). The minor differences in the tracer uptake are erased within 10 minutes as the tracer underwent rapid washout from all analyzed brain regions with the SUVs decreasing below 0.5 within 20 minutes after injection. Consistent with its lower CNS MPO score, [^{11}C]UCM1014 showed a poorer brain uptake at the baseline scan (global SUV_{max} = 1.75, n = 1) compared to [^{11}C]UCM765 and, therefore, was not evaluated in further blocking studies (Figure 4).

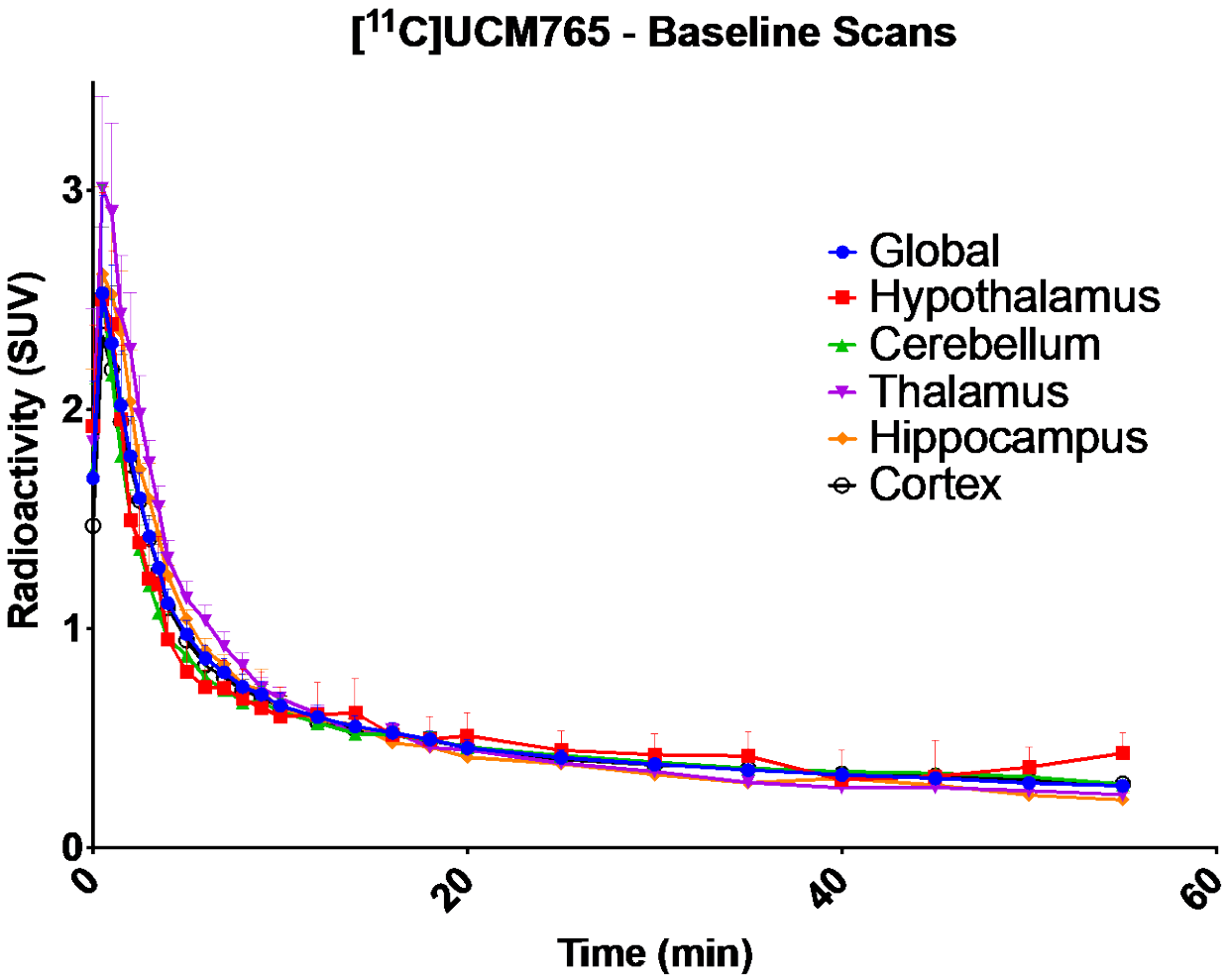

Figure 3. Time-activity curve of the brain regional uptake of [^{11}C]UCM765 in wild-type Sprague-Dawley rats (n = 4)

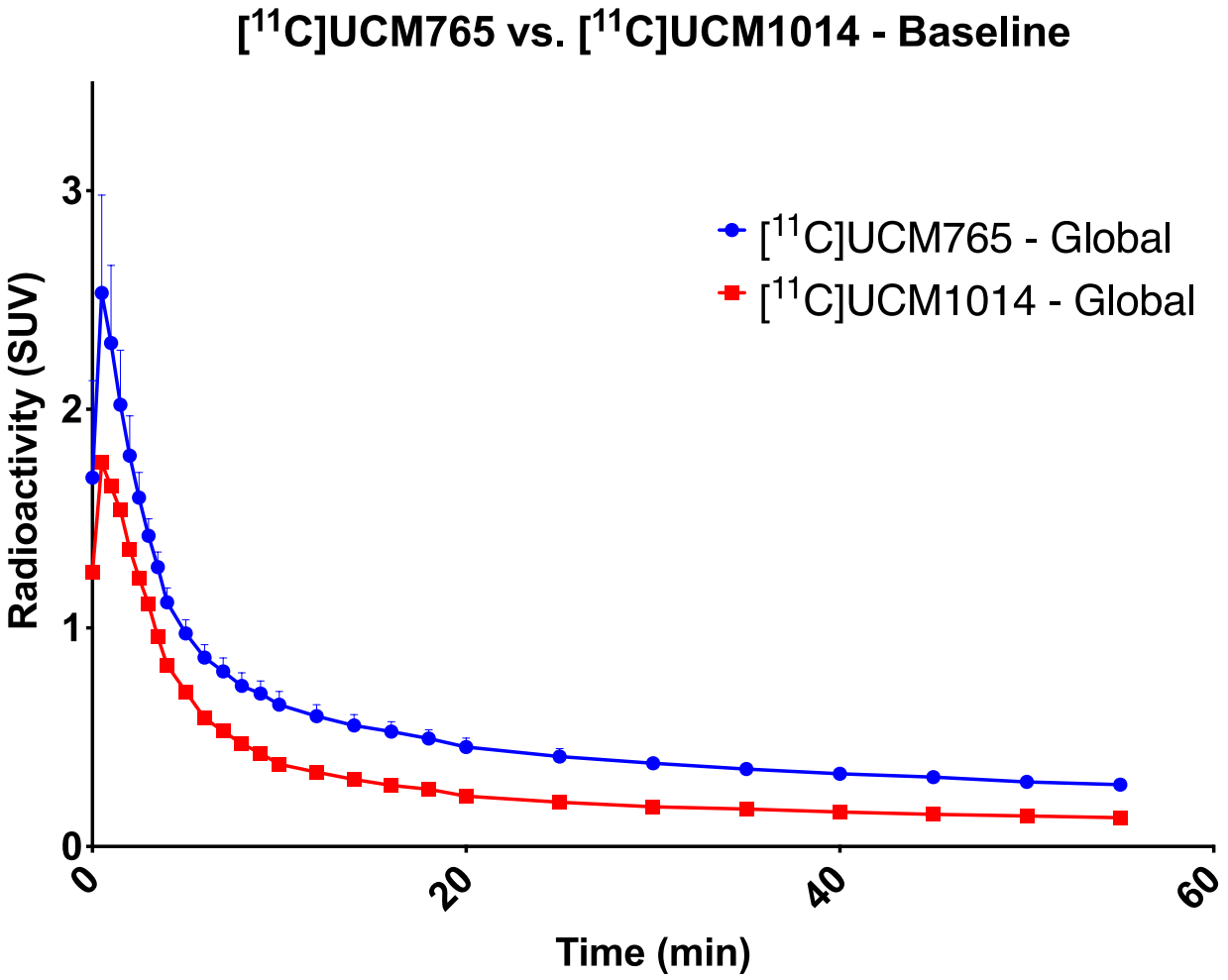

Figure 4. Time-activity curves of global cerebral uptake of [^{11}C]UCM765 (blue; n = 4) and [^{11}C]UCM1014 (red; n = 1) in wild-type Sprague-Dawley rats.

Next, we performed a series of *in vivo* blocking experiments by injecting either selective MT_2 antagonist 4P-PDOT (10 mg/kg, s.c., n = 1) shown to be competitive with UCM765,[41] synthetic MLT (150 mg/kg, s.c., n = 1) or nonradioactive UCM765 (20 mg/kg, i.v., n = 1) prior to the injection of [^{11}C]UCM765 (Figure 5). No significant reduction of the brain uptake has been observed with 4P-PDOT, whereas administration of MLT resulted in a slight reduction in tracer brain uptake in the first 5 minutes of the scan, which can be attributed to restricted cerebral blood flow due to the excessive dose of the administered MLT (150 mg/kg).[47] A homologous blocking

experiment surprisingly resulted in higher apparent tracer brain uptake compared to the baseline scan. We hypothesize that UCM765 is a substrate of metabolic enzymes and saturating those enzymes with non-radioactive compound results in a longer apparent half-life of [^{11}C]UCM765, or a competitive binding occurs at the extracerebral sites of MT_2 expression. Accordingly, the tracer remains longer in the blood circulation and increases the apparent radioactivity signal from the brain. This observation is in accordance with a previously reported short half-life of the parent compound *in vitro* in the presence of rats microsomes ($t_{1/2}$ = 1.7 min).[48]

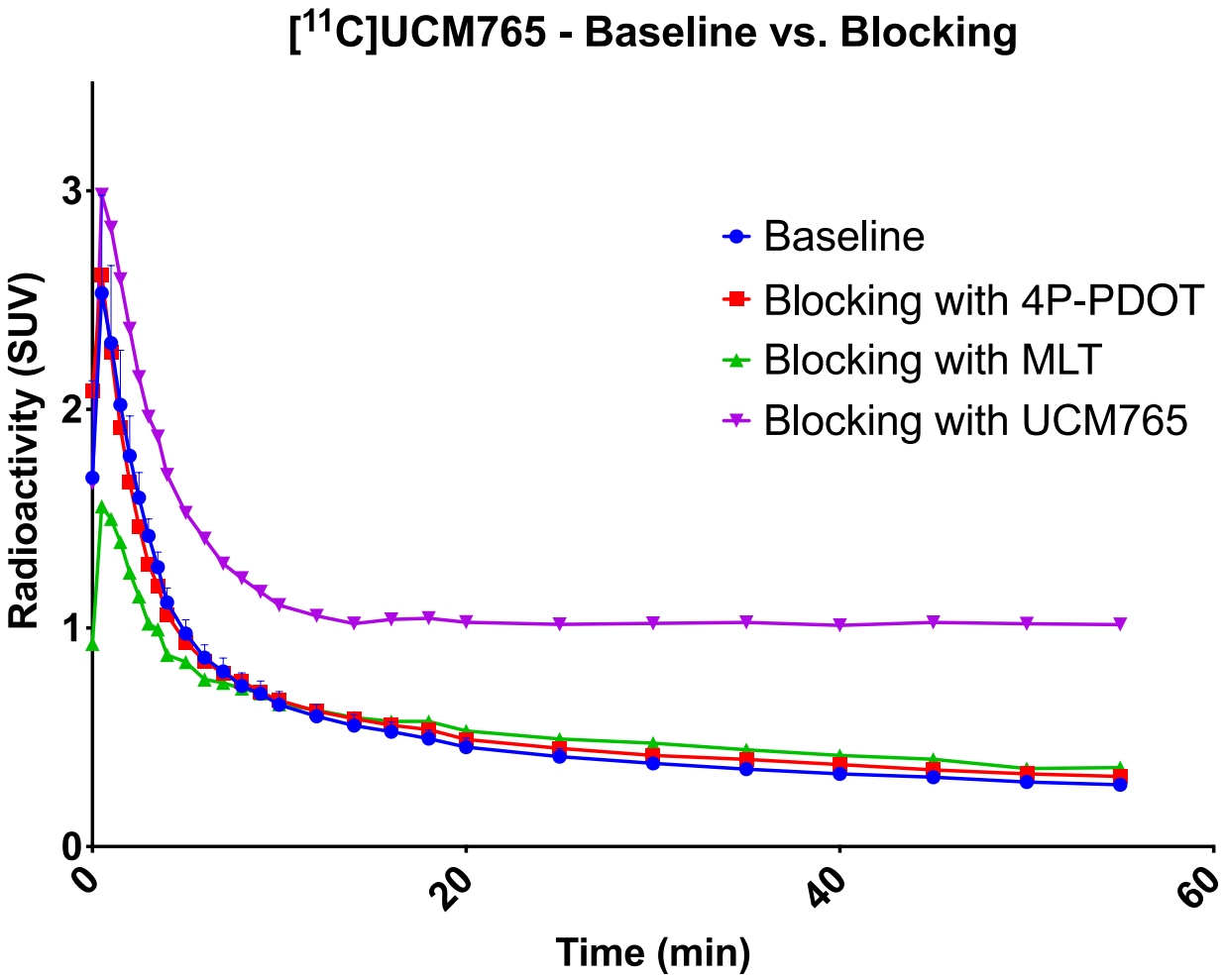

Figure 5. Time-activity curve of the brain regional uptake of [^{11}C]UCM765 cerebral uptake following an injection of saline (blue, s.c., n = 4), 4P-PDOT (red, 10 mg/kg, s.c., n = 1), MLT (green, 150 mg/kg, s.c., n = 1), or nonradioactive UCM765 (purple, 20 mg/kg, i.v., n = 1) in wild-type Sprague-Dawley rats.

We then evaluated two ^{18}F-fluorinated agomelatine derivatives [^{18}F]3FAGM and [^{18}F]FAAGM as PET tracer candidates for non-selective imaging of MT_1 and MT_2 in wild-type Sprague-Dawley rats. Both tracers showed excellent brain permeability within 1 minute after tail-vein injection with a global SUV_{max} of 3.25 ± 0.35 (n = 4) for [^{18}F]3FAGM (Figures 6) and 4.47 ± 0.22 (n = 2) for [^{18}F]FAAGM (Figures 7). Similar to baseline [^{11}C]UCM765 scans, both tracers showed nearly homogenous distribution in all analyzed brain regions, despite the minor differences in the initial uptake with the highest uptake in the thalamus (SUV_{Th} = 3.89 ± 0.51 and 4.67 ± 0.18 for [^{18}F]3FAGM and [^{18}F]FAAGM, respectively) and the lowest uptake in the cortex (SUV_{Ctx} = 2.91 ± 0.33 and 3.93 ± 0.48 for [^{18}F]3FAGM and [^{18}F]FAAGM, respectively). Also similar to [^{11}C]UCM765 scans, uptake of both [^{18}F]3FAGM and [^{18}F]FAAGM was followed by a rapid washout from all analyzed brain regions.

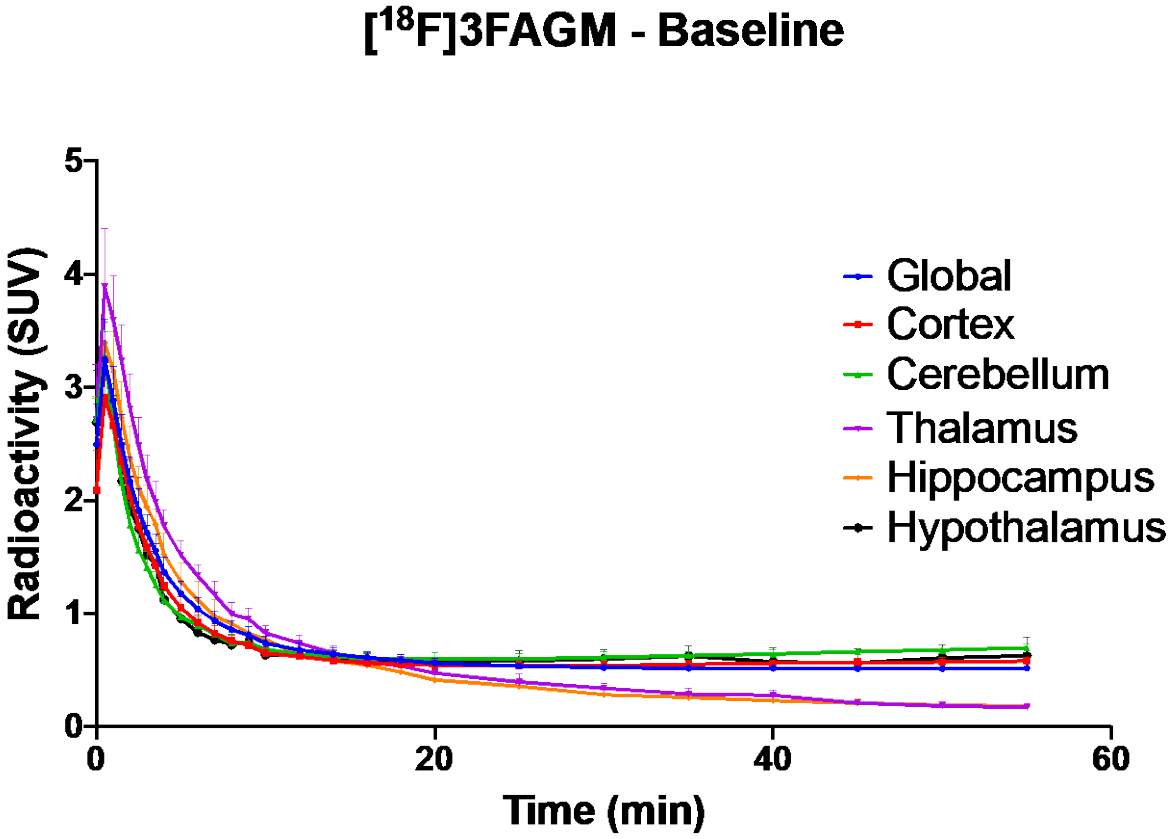

Figure 6. Time-activity curve of the brain regional uptake of [^{18}F]3FAGM in wild-type Sprague-Dawley rats (n = 4)

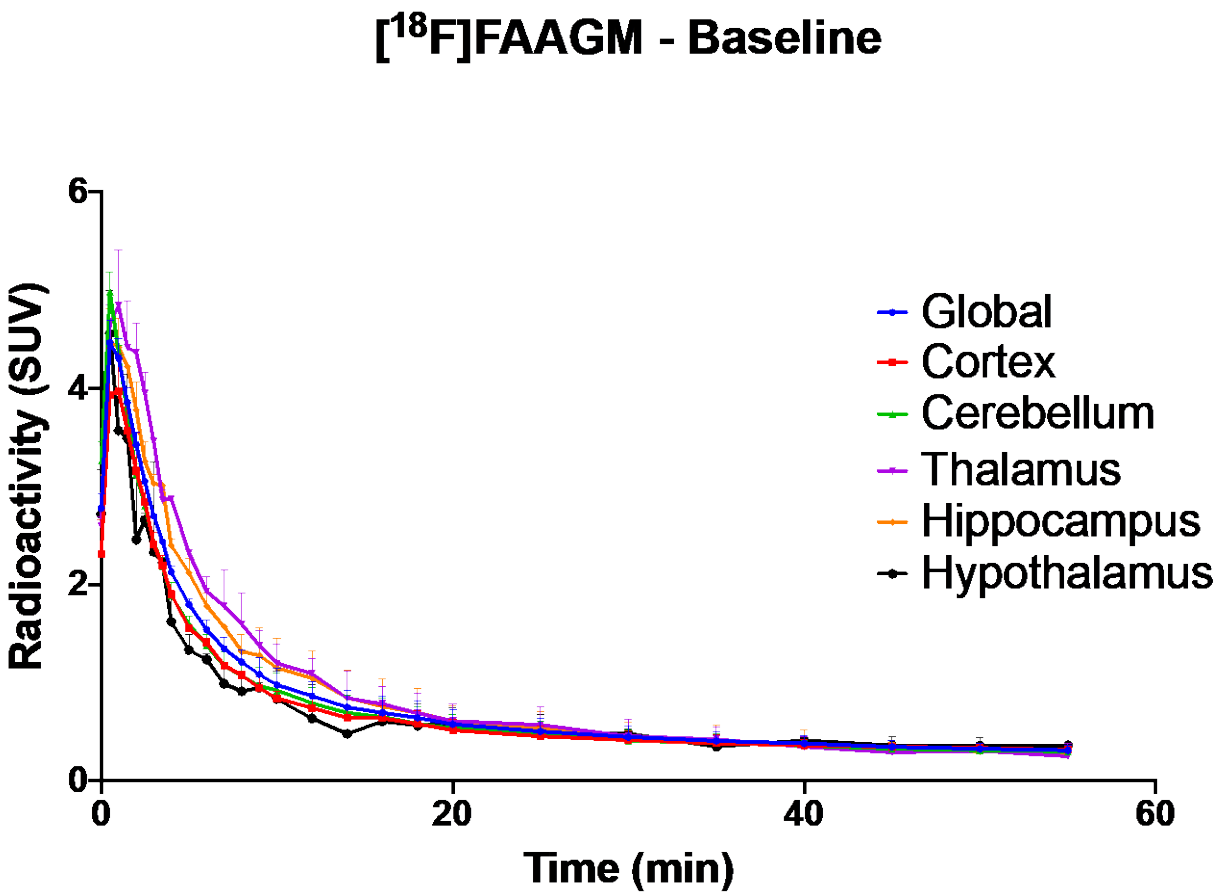

Figure 7. Regional baseline cerebral uptake of [^{18}F]FAAGM in wild-type Sprague-Dawley rats (*n* = 2)

Blocking experiments with either agomelatine (10 mg/kg, s.c., *n* = 2 for [^{18}F]3FAGM, *n* = 2 for [^{18}F]FAAGM) or MLT (150 mg/kg, s.c., *n* = 2 for [^{18}F]3FAGM) does not affect SUV_{max}, but leads to higher retention of both tracers in the later frames of the scans in rats (Figures 8 and 9). However, neither agomelatine- nor MLT-induced increase in the global retention of [^{18}F]3FAGM and [^{18}F]FAAGM were statistically significant ($0.05 < p < 0.1$). At regional level, the uptake of [^{18}F]3FAGM was significantly higher in the cortex, cerebellum, thalamus and hippocampus following agomelatine administration. Similarly, a significant agomelatine-induced increase in [^{18}F]FAAGM uptake was observed in the thalamus and hippocampus. These results could be

attributed to the fact that [^{18}F]3FAGM and [^{18}F]FAAGM are substrates to hepatic microsomal enzymes, where the latter were saturated by agomelatine, which had led to higher regional uptake of these two tracers. MLT, on the other hand, did not show statistically significant changes in [^{18}F]3FAGM retention, neither globally nor regionally.

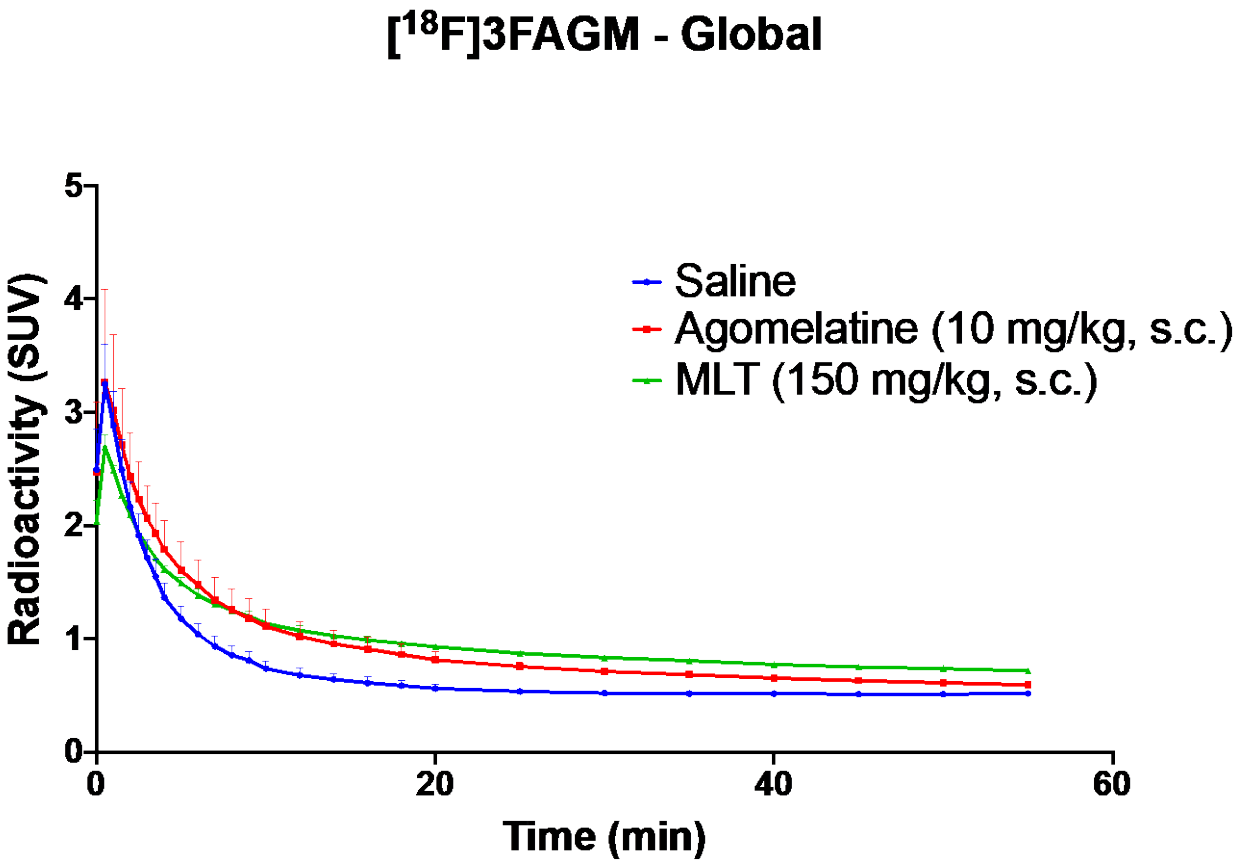

Figure 8. Blocking of [^{18}F]3FAGM with either agomelatine (n = 2) or melatonin (n = 2) does not result in reduced tracer uptake in wild-type Sprague-Dawley rats.

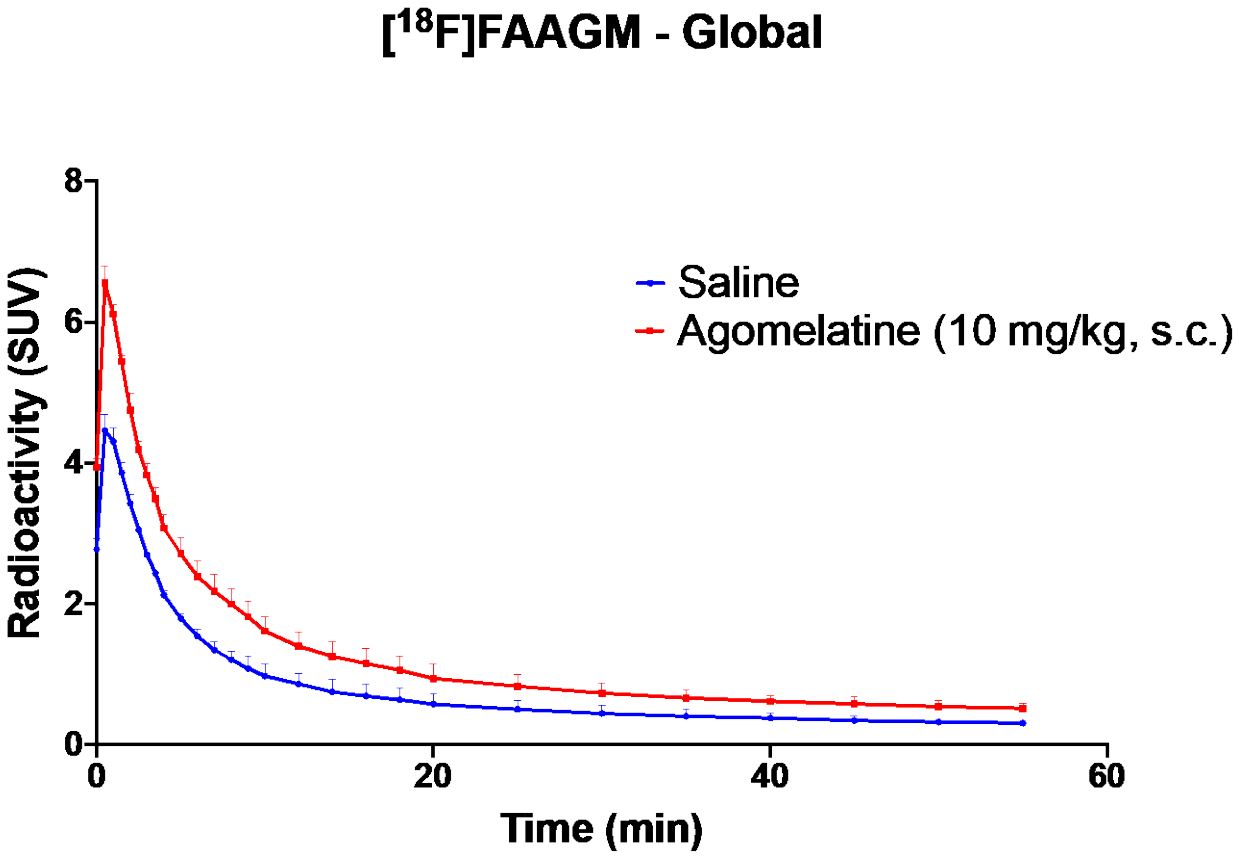

Figure 9. Blocking of [^{18}F]FAAGM with agomelatine (n = 2) does not result in reduced tracer uptake in wild-type Sprague-Dawley rats.

PET imaging in non-human primates. To further evaluate these tracers in higher species, both [^{18}F]3FAGM and [^{18}F]FAAGM were advanced to PET studies in non-human primates. In good correlation with scans in rodents, [^{18}F]FAAGM showed higher brain permeability (SUV_{max} = 3.39 ± 0.06, n = 2) than [^{18}F]3FAGM (SUV_{max} = 2.37, n = 1) in macaques and, therefore, was brought forward to blocking studies using agomelatine (i.v. 4 mg/kg, n = 2). Using cerebellum white matter as a reference region devoid of melatonin receptor expression,[28] we analyzed Logan Distribution Volume Ratios (DVR's) in all other brain regions reported to express either MT_1 and MT_2 including pituitary gland, hypothalamus, thalamus, cerebellum gray matter and basal ganglia. The slope of the Logan plot was estimated using the time period from 5 to 120 min. At the baseline,

$DVR_{5\text{-}120}$ in all regions were below 1 (pituitary gland: 0.78 ± 0.07, hypothalamus: 0.76 ± 0.10, thalamus: 0.97 ± 0.05, cerebellum gray matter: 0.79 ± 0.01 and basal ganglia: 0.74 ± 0.04), suggesting a preferential non-specific binding of the tracer to a white matter (Figure 10). In addition, no statistically significant blocking has been detected in any of the analyzed regions ($\Delta DVR_{5\text{-}120}$ as follows: pituitary gland: −6.9 ± 24.2 %, hypothalamus: −2.3 ± 3.0 %, thalamus: 2.4 ± 4.2 %, cerebellum gray matter: −2.7 ± 2.7 % and basal ganglia: 1.6 ± 1.2 %).

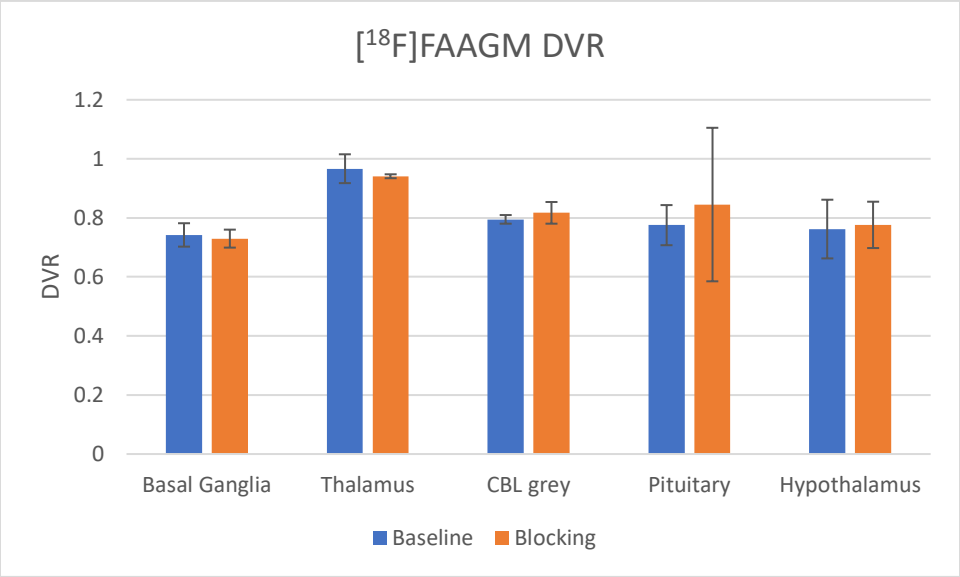

Figure 10. DVR's of [^{18}F]FAAGM in 5 different brain regions with cerebellum white matter as a reference region show preferential accumulation of the tracer in the white matter and a lack of specific binding in blocking experiments (n = 2) with agomelatine (4 mg/kg) in rhesus monkeys.

Autoradiography. Finally, we performed a series of autoradiography experiments on rat and human brain slices using one tracer from each class of lead molecules: [^{11}C]UCM765 and [^{18}F]FAAGM. No preferential binding of [^{11}C]UCM765 in the brain regions reported to express MT_2 was observed. Furthermore, none of 4P-PDOT, MLT or UCM765 (10 μM) reduced the tracer binding in any of the analyzed brain regions (Figures S5-S7). On the other hand, baseline autoradiography

with [^{18}F]FAAGM on human brain tissues showed excessive binding in regions rich with white matter, such as cerebellum white matter, consistent with the *in vivo* PET data. Coincubation with either melatonin (10 µM) or agomelatine (10 µM) did not reduce the tracer binding in any of the analyzed brain regions, including midbrain, hippocampus, pituitary gland and cerebellum (Figure S8). As an example, the ratio of tracer accumulation in the cerebellum grey matter to cerebellum white matter was 0.29, while the blocking in the cerebellum grey matter was not statistically significant with both melatonin (5.2 ± 9.8 %) and agomelatine (4.7 ± 6.7 %).

In vitro biological assays. In order to further investigate the failure of our candidates to specifically detect the expression of melatonin receptors both in PET and in autoradiography studies, we performed a series of *in vitro* biological assays, including measurements of logD, microsomal stability (rat), plasma protein binding (rat) and bidirectional permeability assessment of P-gp efflux susceptibility (MDCK-mdr1 transfected line). The results of these assays are summarized in table 2.

Table 2. Liver microsomal stability (rat), microsomal clearance, plasma protein binding (rat), $logD_{7.4}$ and bidirectional permeability through MDCK-mdr1 and the efflux ratio of FAAGM and 3FAGM.

Compound	$t_{1/2}$ (min) in liver microsomes (rat)	Qh, %	Plasma Protein Binding, %	$logD_{7.4}$	Efflux Ratio BA/AB
FAAGM	9.3 ± 0.4	79.3	90.0 ± 0.5, %	2.68 ± 0.05	1.3
3FAGM	7.5 ± 0.9	82.6	92.8 ± 0.7, %	2.97 ± 0.01	1.2

The data shows that both compounds have suitable lipophilicity ($logD_{7.4}$ ~ 2.6 – 3.0) and plasma free fraction (f_P ~ 5–10 %) and neither is subjected to P-gp efflux. However, both FAAGM and

3FAGM undergo rapid metabolism in the presence of rat liver microsomes as both compounds show a half-life below 10 minutes and the microsomal clearance of ~80%. This suggests a rapid *in vivo* metabolism of our fluorinated agomelatine tracer candidates, which explains its fast washout from the brain and increased brain exposure upon co-injection with agomelatine as they are likely the substrates of the same drug-metabolizing enzymes. Preferential binding to white matter in autoradiography experiments can be explained by the relatively high, albeit acceptable, lipophilicity of both tracers. We therefore conclude that the agomelatine scaffold is likely not suitable for future PET tracer development efforts for melatonin receptors due to its susceptibility to *in vivo* metabolism.

Conclusions.

We developed the radiosynthesis of four different PET tracer candidates for the imaging of melatonin receptors and evaluated their brain permeability, regional distribution, washout rate and binding specificity in rats. All tracers exhibit moderate to high and rapid brain entry in the baseline experiments with almost homogenous distribution in all analyzed brain regions. Administration of several structurally different melatonin receptor ligands increased brain uptake of all of the investigated tracer candidates. The most brain permeable tracer [^{18}F]FAAGM was advanced to *in vivo* PET imaging in non-human primates, but failed to show binding specificity in any of the analyzed brain regions despite excellent brain permeability, while autoradiography in human brain tissues revealed preferential binding to white matter, not blockable by either agomelatine or melatonin. We conclude that this is likely due to the poor pharmacokinetic properties of our lead molecules, including fast metabolism *in vivo* and excessive non-specific binding due to their suboptimal lipophilicity. Low expression levels of both types of melatonin receptors in mammals in large structures of the brain and small anatomical sizes of the nuclei known to express the

highest density of these receptors (e.g. suprachiasmatic nucleus, median eminence and pars tuberalis) may also contribute to the lack of specific binding of the tracer candidates. In addition, the binding of radioligands to melatonin receptors can be influenced by the fluctuation of their expression during the day-night cycle. While we acquired the data on the microsomal stability of the tracer candidates in the presence of liver microsomes, our study lacks the arterial input function, which prevented us from measuring the concentration of parent tracer in blood during PET scans. This limits our ability to fully interpret the PET imaging data. Although PET imaging can play a valuable role in studies of melatonergic system and drug development for the treatment of sleep, pain and mood disorders, further efforts are required to develop selective melatonin PET tracers with more favorable pharmacokinetic properties, including lower lipophilicity and improved metabolic stability.

Methods.

Chemistry.

General. Unless otherwise stated, all reagents were purchased from commercial sources (Sigma-Aldrich, VWR, and Fisher Scientific) and used without further purification. UCM765 has been kindly provided by Prof. Gilberto Spadoni's lab, University of Urbino, Italy. UCM1014 was synthesized as previously described starting from quinolin-5-ol in a 19% yield over 5 steps.[43] *N*-[2-(3-bromo-7-methoxy-naphthalen-1-yl)ethyl]acetamide was synthesized as previously described by bromination of agomelatine in acetic acid.[44] 3-Fluoroagomelatine has been kindly provided by Prof. Saïd Yous's lab, University of Lille, France.

Flash column chromatography was carried out using silica gel 60 Å (particle size 40–63 μm, Silicycle, Canada) as the stationary phase. Compounds were visualized under UV light;

compounds which could not be visualized with UV light were treated with $KMnO_4$ stain developer. All ^{1}H, ^{13}C, and ^{19}F NMR spectra were recorded on a two-channel Bruker 400 or 500 MHz AVIIIHD instrument with an Ascend magnet equipped with a BBFO+ SmartProbe, at a constant temperature of 298 K. COSY, DEPT, HSQC and HMBC experiments were used to aid structural determination and spectral assignment. Chemical shifts (δ) are reported in parts per million (ppm) and referenced to the residual solvent peak. Coupling constants (J) are reported in hertz (Hz) to the nearest 0.5 Hz. Standard abbreviations indicating multiplicities are given: s = singlet, d = doublet, t = triplet, q = quartet, p = pentet, m = multiplet, br = broad. High resolution mass spectrometry (HRMS) data were obtained on a Bruker Maxis Impact Q-TOF by ESI-MS in positive or negative ionization mode. All chemicals used in this study were shown to be ≥95% pure by means of HPLC or NMR.

N-(2-((3-hydroxyphenyl)(phenyl)amino)ethyl)acetamide (**dmUCM765**).

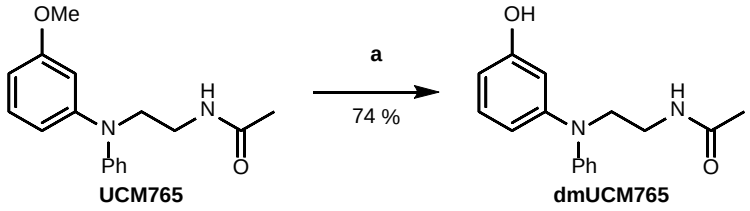

UCM765 (125 mg, 0.44 mmol) was dissolved in 3 mL DCM and cooled to 0 °C. BBr_3 (0.75 mL of 1 M solution in DCM, 1.7 eq.) was added slowly, and the reaction was allowed to warm to room temperature and stirred for 18 h. The mixture was poured into water, neutralized with c. $NaHCO_3$ solution, extracted with 3×50 mL EtOAc, dried over Na_2SO_4, then filtered and the solvent was removed under reduced pressure. The crude product was purified by flash chromatography (silica, 2 % MeOH/DCM) and isolated as 88 mg of pale pink glass in a 74 % yield. ^{1}H NMR (500 MHz, DMSO-d_6) δ 9.22 (s, 1H), 7.96 (t, J = 5.7 Hz, 1H), 7.31 – 7.23 (m, 2H), 7.04 (m, 1H), 7.05 – 6.98

(m, 2H), 6.94 (m, 1H), 6.43 (m, 1H), 6.34 (m, 2H), 3.66 (dd, J = 8.0, 6.5 Hz, 2H), 3.21 (dt, J = 8.2, 6.1 Hz, 2H), 1.77 (s, 3H). ^{13}C NMR (126 MHz, DMSO-d_6) δ 169.5, 158.2, 148.7, 147.4, 129.9, 129.3, 121.3, 121.0, 110.8, 108.4, 107.2, 50.7, 36.3, 22.6. HRMS (ESI+) m/z calcd. for $C_{16}H_{18}N_2NaO_2$ $[M+Na]^+$ 293.1260, found 293.1257.

N-((1-benzyl-5-hydroxy-1,2,3,4-tetrahydroquinolin-2-yl)methyl)propionamide (**dmUCM1014**).

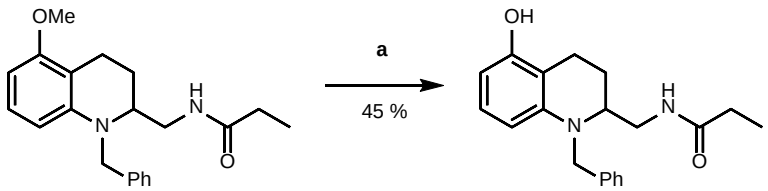

UCM1014 (50 mg, 0.15 mmol) was dissolved in 2 mL DCM and cooled to 0 °C. 0.15 mL BBr_3 (1 M in DCM, 1.7 eq.) was added slowly, and the reaction was allowed to warm to room temperature and stirred for 18 h. The mixture was poured into water, neutralized with c. $NaHCO_3$ solution, extracted 3× with EtOAc, dried over Na_2SO_4, then filtered and the solvent was removed under reduced pressure. The crude product was purified by flash chromatography (silica, 0–10 % MeOH/DCM) and isolated as 20 mg of pale brown glass in a 39 % yield. ^{1}H NMR (500 MHz, DMSO-d_6) δ 8.92 (s, 1H), 7.90 (t, J = 6.0 Hz, 1H), 7.29 (m, 2H), 7.25 – 7.14 (m, 3H), 6.63 (m, 1H), 6.06 (m, 1H), 5.86 (m, 1H), 4.65 – 4.41 (m, 2H), 3.46 – 3.38 (m, 1H), 3.22 (dt, J = 13.1, 5.2 Hz, 1H), 3.06 (ddd, J = 13.2, 9.2, 6.3 Hz, 1H), 2.73 (ddd, J = 17.0, 5.7, 2.2 Hz, 1H), 2.53 – 2.41 (m, 1H), 2.07 (q, J = 7.6 Hz, 2H), 1.95 (m, 1H), 1.70 (m, 1H), 0.99 (t, J = 7.6 Hz, 3H). ^{13}C NMR (126 MHz, DMSO-d_6) δ 173.1, 154.7, 144.6, 139.5, 128.4, 126.5, 126.3, 126.2, 107.4, 102.8, 102.8, 56.3, 53.5, 39.5, 28.5, 21.7, 16.4, 9.9. HRMS (ESI+) m/z calcd. for $C_{20}H_{23}N_2O_2$ $[M-H]^-$ 323.1765, found 323.1768.

2-bromo-*N*-(2-(7-methoxynaphthalen-1-yl)ethyl)acetamide (**BrAAGM**).

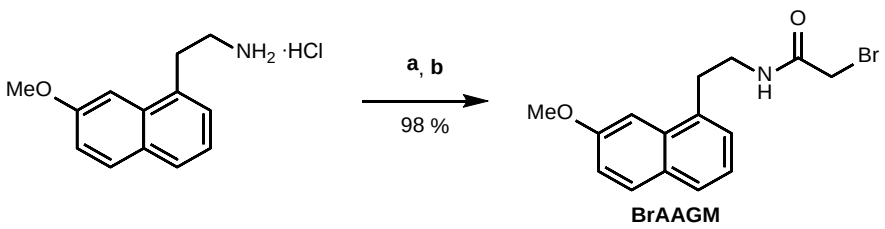

BrAAGM

2-(7-methoxynaphthalen-1-yl)ethan-1-amine hydrochloride (59 mg, 0.25 mmol) was neutralized with saturated $NaHCO_3$ solution, then extracted 2× with $CHCl_3$. The solution was dried over Na_2SO_4, filtered, then the solvent was removed under reduced pressure to yield the free amine, which was used directly. The free amine was redissolved in 5 mL DCM, cooled to 0 °C, then 75 µL of bromoacetyl bromide (1.1 eq.) was added. The solution was warmed to room temperature and stirred for 30 min, then diluted with EtOAc and washed 1× with saturated $NaHCO_3$ and 1× with brine. The organic phase was dried over Na_2SO_4, filtered, then the solvent was removed under reduced pressure. The crude product was purified by flash chromatography (silica, 0–40 % EtOAc/hexanes) to yield 66 mg **BrAAGM** as a white solid in 98 % yield. ^{1}H NMR (500 MHz, $CDCl_3$) δ 7.77 (d, J = 8.9 Hz, 1H), 7.70 (dd, J = 7.6, 1.8 Hz, 1H), 7.45 (d, J = 2.4 Hz, 1H), 7.32 – 7.26 (m, 2H), 7.18 (dd, J = 8.9, 2.5 Hz, 1H), 6.62 (br. s, 1H), 3.99 (s, 3H), 3.86 (s, 2H), 3.69 – 3.63 (m, 2H), 3.28 (t, J = 7.3 Hz, 2H). ^{13}C NMR (126 MHz, $CDCl_3$) δ 165.7, 158.2, 133.2, 133.1, 130.5, 129.5, 127.4, 127.4, 123.3, 118.4, 102.4, 55.6, 40.7, 33.0, 29.3. HRMS (ESI+) m/z calcd. for $C_{15}H_{16}BrNNaO_2$ $[M+Na]^+$ 344.0257, 344.0250.

2-fluoro-*N*-(2-(7-methoxynaphthalen-1-yl)ethyl)acetamide (**FAAGM**).

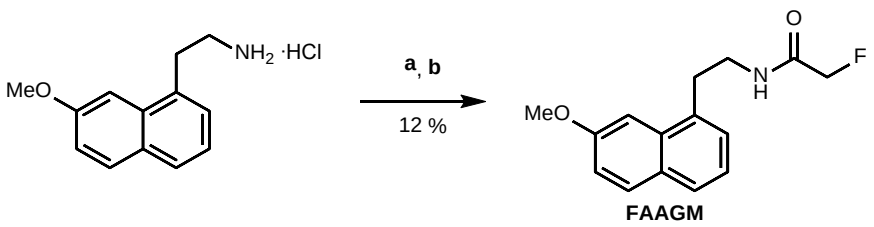

FAAGM

2-(7-methoxynaphthalen-1-yl)ethan-1-amine hydrochloride (115 mg, 0.48 mmol) was neutralized with saturated $NaHCO_3$ solution, then extracted 2× with $CHCl_3$. The solution was dried over Na_2SO_4, filtered, then the solvent was removed under reduced pressure to yield the free amine, which was used directly. The amine was dissolved in 3 mL anhydrous toluene and added to a flask containing 19.1 mg $La(OTf)_3$ (0.05 eq.) and 94.7 µL ethyl fluoroacetate (1.2 eq.) according to the conditions in Reference 49. The solution was heated at 55 °C for 48 h, cooled to room temperature, then loaded directly onto a flash column (silica, 0–40 % EtOAc/hexanes). Pure FAAGM was isolated as 7 mg of white solid in 19 % yield. ^{1}H NMR (500 MHz, $CDCl_3$) δ 7.77 (d, J = 8.9 Hz, 1H), 7.72 – 7.67 (m, 1H), 7.46 (d, J = 2.5 Hz, 1H), 7.34 – 7.27 (m, 2H), 7.18 (dd, J = 9.0, 2.5 Hz, 1H), 6.45 (s, 1H), 4.80 (d, J = 47.4 Hz, 2H), 3.99 (s, 3H), 3.72 (dt, J = 7.9, 6.4 Hz, 2H), 3.30 (t, J = 6.7 Hz, 2H). ^{13}C NMR (126 MHz, $CDCl_3$) δ 168.0 (d, J = 17.0 Hz), 158.2, 133.2, 133.1, 130.5, 129.5, 127.4, 127.3, 123.3, 118.5, 102.4, 80.4 (d, J = 186.0 Hz), 55.6, 39.5, 33.4. ^{19}F NMR (471 MHz, $CDCl_3$) δ −224.68 (td, J = 47.4, 3.3 Hz). HRMS (ESI+) m/z calcd. for $C_{15}H_{16}FNNaO_2$ $[M+Na]^+$ 284.1057, found 284.1057.

N-(2-(7-methoxy-3-(4,4,5,5-tetramethyl-1,3,2-dioxaborolan-2-yl)naphthalen-1-yl)ethyl)acetamide (**3-BpinAGM**).

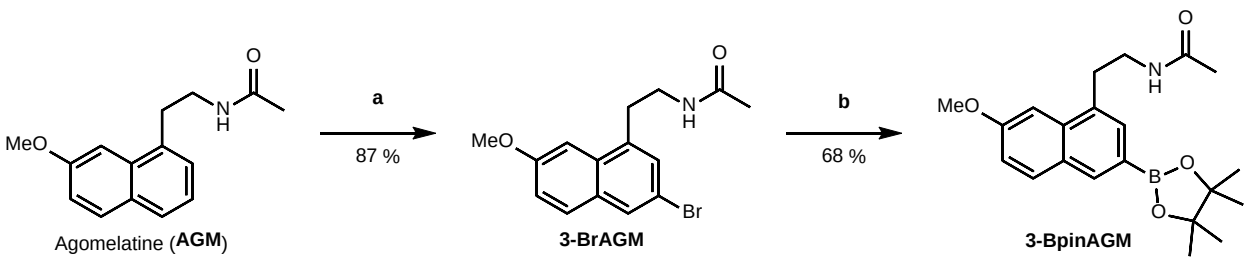

Agomelatine (**AGM**) **3-BrAGM** **3-BpinAGM**

Agomelatine (98 mg, 0.40 mmol) was dissolved in 2 mL HOAc. To this, a solution of 25 µL of Br_2 (1.2 eq.) in 0.25 mL HOAc was added, and the reaction was heated at 70 °C for 6 h. The reaction was cooled to r.t., poured over ice, stirred for 30 minutes, then the resulting solution was extracted 2× with Et_2O, washed once with saturated sodium thiosulfate solution, dried over Na_2SO_4, filtered, and the solvent was removed under reduced pressure. The crude product was purified by flash chromatography (silica, 0–2 % MeOH/DCM) to furnish **3-BrAGM** as 112 mg of off-white powder in an 87 % yield. ^{1}H NMR (500 MHz, $CDCl_3$) δ 7.81 (m, 1H), 7.65 (m, 1H), 7.47 (m, 1H), 7.36 (m, 1H), 7.17 (m, 1H), 5.68 (br. s, 1H), 3.98 (s, 3H), 3.57 (dt, J = 8.5, 6.2 Hz, 2H), 3.21 (t, J = 7.4 Hz, 2H), 1.97 (s, 3H). ^{13}C NMR (126 MHz, $CDCl_3$) δ 170.6, 158.4, 136.2, 132.1, 130.5, 130.1, 129.4, 129.0, 119.7, 116.6, 102.8, 55.7, 40.3, 33.2, 23.5. HRMS (ESI+) m/z calcd. for $C_{15}H_{16}BrNNaO_2$ $[M+Na]^+$ 344.0257, found 344.0254.

A vial was charged with **3-BrAGM** (50 mg, 0.16 mmol), 49 mg B_2pin_2 (1.25 eq.), 23 mg $PdCl_2$dppf (0.2 eq.), 30 mg KOAc (2 eq.). The vial was purged with argon, then 3 mL degassed DMSO was added, and the mixture was heated at 80 °C for 18 h. The reaction was cooled to room temperature, then diluted into water and washed 3× with EtOAc. The organic phase was washed 2× with brine, dried over Na_2SO_4, filtered, and the solvent was removed under reduced pressure. The crude product was purified by flash chromatography (silica, 0–80 % EtOAc/hexanes) to yield **3-BpinAGM** as 39 mg of pale brown solid in a 68% yield. ^{1}H NMR (500 MHz, DMSO-d_6) δ 8.12 (t, J = 6.4 Hz, 1H), 8.11 (s, 1H), 7.92 (d, J = 9.0 Hz, 1H), 7.63 (d, J = 2.5 Hz, 1H), 7.52 (d, J = 1.2

Hz, 1H), 7.17 (dd, J = 8.9, 2.4 Hz, 1H), 3.96 (s, 3H), 3.32 – 3.27 (m, 1H), 3.15 – 3.09 (m, 2H), 1.83 (s, 3H), 1.32 (s, 12H). ^{13}C NMR (126 MHz, DMSO-d_6) δ 169.5, 158.6, 134.8, 134.8, 133.4, 131.3, 131.0, 128.2, 118.2, 102.6, 83.6, 55.4, 39.8, 33.1, 24.8, 22.6. HRMS (ESI+) m/z calcd. for $C_{21}H_{28}BNNaO_4$ $[M+Na]^+$ 392.2004, found 392.2001.

Radiochemistry.

General. All radiosynthesis and quality control procedures were conducted in the cyclotron and radiochemistry facility of the McConnell Brain Imaging Centre (BIC), Montreal Neurological Institute (the Neuro), McGill University (Montreal, Canada) or in the cyclotron and radiochemistry facility of the University of Michigan (Ann Arbor, USA). Unless otherwise stated, reagents and solvents were commercially available and used without further purification: sodium chloride solution, 0.9% USP grade, and sterile water for injection USP grade were purchased from Hospira or Baxter; ethanol was purchased from Commercial alcohols (McGill University) or American Regent (University of Michigan); HPLC grade acetonitrile was purchased from Fisher Scientific. Other synthesis components were obtained as follows: sterile filters were obtained from Millipore; sterile product vials were purchased from Hollister-Stier; QMA-light and C18-light Sep-Paks were purchased from Waters Corporation. Radiosyntheses and HPLC purifications were carried out on the automated radiosynthesis units (Synthra for carbon-11 labelling at McGill University; Scintomics GRP for fluorine-18 labelling at McGill University; GE TRACERLAB FX_{FN} for fluorine-18 labelling at the University of Michigan) equipped with semi-preparative HPLC columns. Collected tracer fractions were diluted with water (15 mL) and loaded on a preconditioned (5 mL ethanol followed by 10 mL water) Sep-Pak C-18 Light cartridge. The cartridge was washed with distilled water (5 mL) and the tracer was eluted with ethanol (0.5 mL) followed by saline (4.5 mL) into a vial. Quality control was performed on analytical HPLC

(Agilent 1200 series at McGill University; Shimadzu Prominence UFLC at the University of Michigan) equipped with UV and radioactivity detectors using either Phenomenex Aeris Peptide XB-C18 (250×4.6mm 3.6 µm), Phenomenex Prodigy ODS-3 (250×4.6 mm, 10 µm) or Phenomenex Luna PFP(2) (150×4.6 mm, 5 µm) columns. Radiotracer identities were confirmed by co-injection with the corresponding non-radioactive standards (Figures S1–S4).

[^{11}C]UCM765 and *[^{11}C]UCM1014*. [^{11}C]Methyl iodide ([^{11}C]CH_3I) was produced *via* the gas phase method and trapped in a solution of a **dmUCM765** or a **dmUCM1014** precursor (1.0–2.0 mg) in DMSO (0.5 mL) containing 5 M NaOH (10 µL), followed by heating at 90 °C for 5 min. The reaction mixture was then diluted with 2 mL of the HPLC eluent and purified on Phenomenex Luna C18 column (100 Å, 250×10 mm, 10 µm) using 20 mM NH_4HCO_2/MeCN (50:50) as an eluent at 4 mL/min flow rate. Quality control HPLC (column: Phenomenex® Aeris PEPTIDE 3.6 µm XB-C18, 250×4.6 mm; eluent: 0.1% TFA/MeCN (35:65); flow rate: 0.7 mL/min; wavelength: 300 nm) confirmed [^{11}C]UCM765 and [^{11}C]UCM1014 were produced with the radiochemical purities (RCP) of >99 % and molar activities (A_m) of 372±60 GBq/µmol. Decay-corrected radiochemical yields (RCY) starting from [^{11}C]CH_3I were as follows: [^{11}C]UCM765 (17–22 %, n = 3); [^{11}C]UCM1014 (18 %, n = 1). The syntheses were completed within 20–25 minutes from the completion of [^{11}C]methyl iodide transfer.

[^{18}F]3FAGM. McGill procedure: [^{18}F]F^-/H_2O (7.4–18.5 GBq) was passed through an unconditioned Sep-Pak Light 46 mg QMA cartridge (Waters) from the male side. The cartridge was then flushed with methanol (3 mL) from the male side and ^{18}F-fluoride was then eluted with 450 µL of a tetraethylammonium bicarbonate solution in methanol (1 mg/mL) followed by methanol (500 µL) from the female side into a conical Wheaton vial (5 mL). The solvent was removed at 100 °C under vacuum, first under a stream of argon (100 mL/min), then in closed

system and the vacuum was quenched with air. The reaction vial was then charged with **3-BpinAGM** precursor (3.7 mg, 10 µmol) and $Cu(OTf)_2py_4$ (6.8 mg, 10 µmol) in a mixture of dimethylacetamide (500 µL) and 1-butanol (250 µL) and the mixture was allowed to react for 20 min at 130 °C. The crude mixture was then cooled to 50 °C, diluted with HPLC eluent (1.5 mL) and purified on Phenomenex Luna PFP(2) column (100 Å, 250×10 mm, 5 µm) using 20 mM NH_4HCO_2/MeCN (65:35) as an eluent at 4 mL/min flow rate (R_t = 33–35 min). The fraction containing purified radiotracer was collected, reformulated as described above and subjected to analytical HPLC procedures (column: Phenomenex Prodigy ODS-3, 250×4.6mm; eluent: 0.1% TFA/MeCN (50:50); flow rate: 0.7 mL/min; wavelength: 230 nm). [^{18}F]3FAGM was obtained within 90 minutes from [^{18}F]F^- in 20.3 ± 6.6 % decay-corrected RCY (n = 2), >99 % RCP and 108.7 ± 47.5 GBq/µmol A_m.

University of Michigan procedure: [^{18}F]Fluoride ion was produced using the $^{18}O(p,n)^{18}F$ nuclear reaction *via* proton bombardment of a $H_2{}^{18}O$ liquid target on a GE PETtrace cyclotron at a beam current of 55 µA for 30 minutes. The [^{18}F]fluoride from 2.5 mL of irradiated ^{18}O-water was trapped on a QMA-light Sep-Pak cartridge (Waters) that had been preconditioned with ethanol (10 mL), 0.5 M KOTf aqueous solution (10 mL) and MilliQ H_2O (10 mL). Fluoride was eluted into the reaction vessel using a solution of tetraethylammonium bicarbonate (0.05 mg) and KOTf (10 mg) in 0.5 mL of water; the fluoride was then treated with acetonitrile (1 mL) and azeotropically dried at 100 °C first under vacuum and then under vacuum and argon overpressure. A solution of **3-BpinAGM** precursor (3.7 mg, 10 µmol) and $Cu(OTf)_2py_4$ (6.8 mg, 10 µmol) in a mixture of DMA (300 µL) and 1-butanol (150 µL) was added and the reaction mixture was heated at 130 °C for 20 min. After cooling to 50 °C, the reaction mixture was diluted with mobile phase (1.5 mL) and purified by semi-preparative HPLC (column: Luna PFP(2) 250×10 mm; mobile phase: 20 mM

NH_4HCO_2/MeCN (65:35) as an eluent at 4 mL/min flow rate). The collected peak was diluted in 50 mL of MQ H_2O for reformulation. The solution was passed over a C18 1 cc Sep-Pak to trap the radiotracer and rinsed with water (5 mL) to remove residual solvent. Elution with USP ethanol (1 mL) of the radiotracer into the collection vial was followed by rinsing of the Sep-Pak with saline (9 mL) to achieve a 10% ethanol in saline dose formulation that was passed through a sterile filter into a sterile vial prior to quality control analysis and use in imaging studies. Overall synthesis time was 105 minutes from end-of-bombardment. Decay corrected product yield: 7.95 ± 0.77 GBq (n = 2), RCY = 11.5%, A_m = 159.89 GBq/μmol.

[^{18}F]FAAGM. McGill procedure: [^{18}F]F^-/H_2O (7.4–18.5 GBq) was passed through a Sep-Pak Light Carbonate QMA cartridge (Waters), preconditioned with 10 mL water. [^{18}F]fluoride was then eluted with a mixture of aqueous K_2CO_3 (0.125M, 150 μL), K222 (10-12 mg) and acetonitrile (~ 1 mL) into a conical Wheaton vial (5 mL). The solvent is azeotropically removed at 100 °C under vacuum and a stream of argon (100 mL/min), followed by two additional azeotropic drying steps with 0.5 mL acetonitrile added each time. The reaction vial was then charged with **BrAAGM** precursor (4.5 mg, 14 μmol) in acetonitrile (500 μL) and the mixture was heated for 15 min at 100 °C. The crude mixture was then cooled, diluted with HPLC eluent (1.5 mL) and purified on a Phenomenex Luna C18 column (100 Å, 250 × 10 mm, 10 μm) using 20 mM NH_4HCO_2/MeCN (60:40) at 4 mL/min flow rate (R_t = 24–26 min). The fraction containing purified radiotracer was collected, reformulated as described above and subjected to analytical HPLC procedures (column: Phenomenex Prodigy ODS-3, 250×4.6mm; eluent: MeCN/H_2O (60:40); flow rate: 1.0 mL/min; wavelength: 230 nm). [^{18}F]FAAGM was obtained within 90 minutes from [^{18}F]F^- in 10.7 ± 6.6 % decay-corrected RCY (n = 2), >99% RCP and 281.9 ± 147.5 GBq/μmol A_m (*n* = 2).

University of Michigan procedure: [^{18}F]Fluoride ion was produced using the ^{18}O(p,n)^{18}F nuclear reaction *via* proton bombardment of a $H_2{}^{18}O$ liquid target on a GE PETtrace cyclotron at a beam current of 55 μA for 30 minutes. The [^{18}F]fluoride from 2.5 mL of irradiated ^{18}O-water was trapped on a QMA-light Sep-Pak cartridge (Waters) that had been preconditioned with ethanol (10 mL), 0.5 M $NaHCO_3$ aqueous solution (10 mL) and MilliQ H_2O (10 mL). Fluoride was eluted into the reaction vessel using an aqueous solution of K_2CO_3 (3.5 mg in 0.5 mL of water), and then crypt-222 (15 mg in 1.0 mL of acetonitrile) was added so the fluoride could be azeotropically dried at 100 °C first under vacuum and then under vacuum and argon overpressure. A solution of **BrAAGM** precursor (4.5 mg) in anhydrous acetonitrile (400 μL) was added to the dried fluoride in the reactor, and the solution was heated at 100 °C for 15 min. After cooling to 50 °C, the reaction mixture was diluted with mobile phase (1.5 mL) and purified by semi-preparative HPLC (column, Luna PFP(2) 250 × 10 mm; mobile phase, 20 mM NH_4HCO_2/MeCN (65:35) eluent at 4 mL/min flow rate). The collected product was diluted in MQ H_2O (50 mL) transferred across a C18 1 cc Sep-Pak to trap the radiotracer and rinsed with water (5 mL) to remove residual solvent. The product was eluted with ethanol (1 mL) and the Sep-Pak was rinsed with saline (9 mL) to give a 10% ethanol saline formulated dose that was passed through a sterile filter into a sterile vial prior to quality control analysis and use in imaging studies. Overall synthesis times were 90 minutes after end-of bombardment. Decay corrected product yield: 0.43 ± 0.31 GBq, RCY = 0.93 %, n = 6, A_m = 45.1 GBq/μmol.

PET imaging in rats.

All experimental procedures were approved by the McGill University Animal Care Committee (UACC, protocol #2017-7914) and were in compliance with the guidelines of the Canadian Council on Animal Care (CCAC). Male *Sprague Dawley* rats (300–400 g, 6–9 weeks old) were

purchased from Charles River Canada for microPET imaging experiments. All PET images were acquired using a CTI Concorde R4 microPET scanner for small animals (CTI, Siemens, Munich, Germany) between 11 a.m. and 3 p.m. (Zeitgeber time = 6 – 10 hours). Anesthesia was first induced using isoflurane at 5% with 2–3 L/min oxygen flow, then maintained for the duration of the scan at 1.5–2.5% isoflurane with 0.8 L/min oxygen flow. The rat brain was positioned at the center of field of view (FOV) and the 60-minute dynamic scan was acquired in 27 frames (8×30 s, 6×1 min, 5×2 min, 8×300 s) concomitantly with the bolus injection of the tracer in 10 % ethanol saline in the tail vein. The mean injected tracer activity was 17.5 MBq and mean injected volume was 0.7 mL. Each emission scan was either preceded (for ^{18}F-labelled tracers) or followed (for ^{11}C-labelled tracers) by a 9-minute transmission scan with a ^{57}Co point source to correct for attenuation. In blocking experiments, a solution of the competitor was injected either subcutaneously 7–10 min prior to the tracer injection (4P-PDOT, melatonin or agomelatine) or intravenously immediately before tracer injection (nonradioactive UCM765). MRI structural images for co-registration purposes were obtained using a 7 T Bruker Pharmascan pre-clinical MRI system, with a Bruker volume resonator radiofrequency (RF) coil designed for rat brain imaging. Images were reconstructed using the *Maximum A Posteriori* (MAP) algorithm and corrected for attenuation, scatter, dead time and decay. Imaging processing and analyses were conducted using MINC tools (www.bic.mni.mcgill.ca/ServicesSoftware). Both eyes, nose bone and base of the skull were used as landmarks to co-register the PET to MRI images. Atlas-based auto-segmentation of the regions of interests (ROI's) was performed with ITK-SNAP (v. 3.6.0; http://www.itksnap.org/pmwiki/pmwiki.php),[50] based on brain region delineations reported in the Waxholm Space atlas of the Sprague Dawley rat brain (https://www.nitrc.org/projects/whs-sd-

atlas).[51] Radioactivity counts were normalized to the amount of injected activity and animal weight and the results were expressed as Standardized Uptake Value (SUV).

$$SUV = \frac{Radioactivity\ Counts * Body\ Weight\ (g)}{Injected\ Dose\ (Bq)}$$

PET Imaging in non-human primates.

All primate imaging studies were performed in accordance with the standards set by the University Committee on Use and Care of Animals (UCUCA) at the University of Michigan. Imaging was done in two intact mature female rhesus monkeys (*Macaca mulatta*, body weight = 9.06–9.72 kg with negligible variation throughout the duration of the study) using the Concorde Microsystems MicroPET P4 tomograph (Knoxville, TN) between 10 a.m. and 12 p.m. (Zeitgeber time = 4–6 hours). The animals were anesthetized in the home cage with Telazol and transported to the PET facility. Subjects were intubated for mechanical ventilation, and anesthesia was continued with isoflurane. Anesthesia was maintained throughout the duration of the PET scan. A venous catheter was inserted into one hind limb and the monkey was placed on the PET gantry with its head secured to prevent motion artefacts. Ten minutes later, 0.16–0.17 GBq of [^{18}F]FAAGM or [^{18}F]3FAGM was administered in a bolus dose over 1 minute, and the brain scan acquisition started concomitantly for 120 min. Emission data were collected in 19 frames (5×1 min, 2×2.5 min, 2×5 min, 10×10 min). Collection of vitals (HR, SPO_2, $EtCO_2$ and respiratory rate) was carried out during the whole scan. For the blocking scans, agomelatine (3.5 mg/mL formulation in 6.6 % ethanol and 1.6 % Tween-80 in saline) was passed through a sterile filter and injected intravenously at 4 mg/kg dose immediately (no more than 10 minutes) before injection of radiotracer. Emission data were corrected for attenuation and scatter, and reconstructed using the 3D maximum a priori method (3D MAP algorithm). PET scans were registered to an existing FDG

monkey PET scan from the University of Michigan PET facility using SPM (https://www.fil.ion.ucl.ac.uk/spm/doc/). The regions defined previously on a variety of PET radiotracer scans, including FDG, flumazenil, and carfentanil, were applied to the scans reported in this paper. Using a summed image of the entire data set, regions of interest (ROIs) were drawn by alignment with NIMH macaque brain atlas (https://afni.nimh.nih.gov/pub/dist/doc/htmldoc/nonhuman/macaque_tempatl/template_nmtv2.html) per published methods.[52] Data from multiple planes was obtained for volumetric ROIs for the whole brain, thalamus, hypothalamus, pituitary gland, cerebellum gray and white matter and basal ganglia. The volumetric ROIs were then applied to the full dynamic data sets to obtain the regional tissue time-radioactivity data.

Autoradiography

Human brain tissues were acquired from the Douglas-Bell Canada Brain Bank and used under approved protocol #IUSMD-20-02 to Dr. Rosa-Neto. Rat brain tissues were acquired from the sacrificed male Long-Evans rats (400–500 g, 11 months old, Charles River Canada) by decapitation and extraction followed by the rapid freezing of the brains under approved protocol #7301 to Dr. Rosa-Neto. The tissues frozen to −80 °C were sliced to 20 µm thickness and mounted onto Superfrost Plus slides (Thermo Scientific). The aqueous buffer was prepared from a solution of NaCl (138 mM) and KCl (2.7 mM) by adjusting the pH to 7.4 with NaOH and adding Bovine serum albumin (1%). After thawing and pre-incubation in either buffer (17 mL) or a blocking solution (10 µM, 17 mL) for 1 hour, solution of radiotracer was added to bring the radioactivity concentration to 37 kBq/mL and the slides were incubated in the tracer solution with or without competitor for an additional 40 minutes (for ^{11}C-labelled tracers) or 2.5 hours (for ^{18}F-labelled tracers). After a rinse with cold buffer (3×3 minutes, 0 °C) followed by cold water (30 s, 0 °C), the

labeled slices were dried and placed on phosphor-imaging plates with industrial tritium activity standards. After exposure for 20 minutes, the plates were scanned with a plate reader (BAS 5000; Fuji or Typhoon Trio + Variable Mode Imager).

In vitro biological assays

Plasma protein binding, stability in the presence of rat liver microsomes, $logD_{7.4}$ and bidirectional permeability assessment in MDCK-mdr1 transfected line of 3FAGM and FAAGM was performed at the contract research organization (CRO) Paraza Inc. following standard protocols.

Statistical Analyses

A 2-way paired sampled t-test was conducted using SPSS software to determine the difference between saline- and blocking agent (agomelatine or MLT)-induced changes in the area under curve (AUC) of tracers' uptake.

Author Contributions

[§] H.B. and T.A.S. contributed equally.

[§§] A.F.B and A.K. contributed equally.

A.K., H.B. and G.G. conceived of the project. J.-P.S. and C.B. contributed to concept and design of study. A.K., P.J.H.S. and A.F.B. managed the study. T.A.S., G.S., A.B. and S.Y. performed organic synthesis. H.B., T.A.S., A.K., D.J., A.F.B. and T.K. performed radiochemistry and quality control. K.R., A.A., D.R. and H.B. performed the imaging studies in rats. A.F.B. and T.K. performed the imaging studies in non-human primates. A.A. performed the autoradiography. H.B., P.R-N. and M.S.K. processed images and performed the PET data analysis in rats. A.F.B. and R.K. processed images and performed the PET data analysis in non-human primates. A.K., T.A.S., H.B. and A.F.B. wrote the manuscript.

Funding

This work is supported by the Alzheimer Society of Canada Grant 18-05 (to A.K.), the Quebec Bio-Imaging Network Grant 35450 (to A.K. and G.G.), the National Institutes of Health Grant R01EB021155 (to P.J.H.S.), the Canadian Institutes of Health Research (CIHR) Grant FRN 152985 (to P.R-N.), the Alzheimer's Association Grant NIRP-12-259245 (to P.R-N.), Fonds de Recherche du Québec – Santé (FRQS) Chercheur Boursier 2020-VICO-279314 (to P.R-N.). McConnell Brain Imaging Centre is also supported by the Brain Canada Foundation with support from Health Canada.

Notes

The authors declare no competing financial interest.

Supporting information

The Supporting Information is available free of charge at …

Synthetic procedures, characterization details of new compounds, representative HPLC chromatograms, PET images and autoradiography data.

Acknowledgments

Authors thank Robert Hopewell, I-Huang Tsai, Marina Kostikova and Monica Samoila for access to medical radioisotopes and assistance with tracer radiosynthesis and quality control. Authors thank Paraza Inc. for performing in vitro biological assays on tracer candidates.

References

(1) Brzezinski, A. Melatonin in Humans. *N. Engl. J. Med.* **1997**, *336* (3), 186–195. https://doi.org/10.1056/NEJM199701163360306.

(2) Hardeland, R.; Cardinali, D. P.; Srinivasan, V.; Spence, D. W.; Brown, G. M.; Pandi-Perumal, S. R. Melatonin—A Pleiotropic, Orchestrating Regulator Molecule. *Prog. Neurobiol.* **2011**, *93* (3), 350–384. https://doi.org/10.1016/j.pneurobio.2010.12.004.

(3) Lacoste, B.; Angeloni, D.; Dominguez-Lopez, S.; Calderoni, S.; Mauro, A.; Fraschini, F.; Descarries, L.; Gobbi, G. Anatomical and Cellular Localization of Melatonin MT_1 and MT_2 Receptors in the Adult Rat Brain. *J. Pineal Res.* **2015**, *58* (4), 397–417. https://doi.org/10.1111/jpi.12224.

(4) Klosen, P.; Lapmanee, S.; Schuster, C.; Guardiola, B.; Hicks, D.; Pevet, P.; Felder-Schmittbuhl, M. P. MT_1 and MT_2 Melatonin Receptors Are Expressed in Nonoverlapping Neuronal Populations. *J. Pineal Res.* **2019**, e12575. https://doi.org/10.1111/jpi.12575.

(5) Gobbi, G.; Comai, S. Differential Function of Melatonin MT_1 and MT_2 Receptors in REM and NREM Sleep. *Front. Endocrinol. (Lausanne).* **2019**, *10*. https://doi.org/10.3389/fendo.2019.00087.

(6) Comai, S.; Gobbi, G. Unveiling the Role of Melatonin MT_2 Receptors in Sleep, Anxiety and Other Neuropsychiatric Diseases: A Novel Target in Psychopharmacology. *J. Psychiatry Neurosci.* **2014**, *39* (1), 6–21. https://doi.org/10.1503/jpn.130009.

(7) Savaskan, E.; Ayoub, M. A.; Ravid, R.; Angeloni, D.; Fraschini, F.; Meier, F.; Eckert, A.; Muller-Spahn, F.; Jockers, R. Reduced Hippocampal MT_2 Melatonin Receptor Expression

in Alzheimer's Disease. *J. Pineal Res.* **2005**, *38* (1), 10–16. https://doi.org/10.1111/j.1600-079X.2004.00169.x.

(8) Brunner, P.; Sözer-Topcular, N.; Jockers, R.; Ravid, R.; Angeloni, D.; Fraschini, F.; A., E.; Müller-Spahn, F.; Savaskan, E. Pineal and Cortical Melatonin Receptors MT_1 and MT_2 Are Decreased in Alzheimer's Disease. *Eur. J. Histochem.* **2006**, *50* (4), 311–316. https://doi.org/10.4081/1002.

(9) Adi, N.; Mash, D. C.; Ali, Y.; Singer, C.; Shehadeh, L.; Papapetropoulos, S. Melatonin MT_1 and MT_2 Receptor Expression in Parkinson's Disease. *Med. Sci. Monit.* **2010**, *16* (2), BR61-67.

(10) Wang, X.; Sirianni, A.; Pei, Z.; Cormier, K.; Smith, K.; Jiang, J.; Zhou, S.; Wang, H.; Zhao, R.; Yano, H.; Kim, J. E.; Li, W.; Kristal, B. S.; Ferrante, R. J.; Friedlander, R. M. The Melatonin MT_1 Receptor Axis Modulates Mutant Huntingtin-Mediated Toxicity. *J. Neurosci.* **2011**, *31* (41), 14496–14507. https://doi.org/10.1523/JNEUROSCI.3059-11.2011.

(11) Liu, J.; Clough, S. J.; Hutchinson, A. J.; Adamah-Biassi, E. B.; Popovska-Gorevski, M.; Dubocovich, M. L. MT_1 and MT_2 Melatonin Receptors: A Therapeutic Perspective. *Annu. Rev. Pharmacol. Toxicol.* **2016**, *56* (1), 361–383. https://doi.org/10.1146/annurev-pharmtox-010814-124742.

(12) Pévet, P. Melatonin Receptors as Therapeutic Targets in the Suprachiasmatic Nucleus. *Expert Opin. Ther. Targets* **2016**, *20* (10), 1209–1218. https://doi.org/10.1080/14728222.2016.1179284.

(13) Auld, F.; Maschauer, E. L.; Morrison, I.; Skene, D. J.; Riha, R. L. Evidence for the

Efficacy of Melatonin in the Treatment of Primary Adult Sleep Disorders. *Sleep Med. Rev.* **2017**, *34*, 10–22. https://doi.org/10.1016/j.smrv.2016.06.005.

(14) Kostiuk, N. V.; Belyakova, M. B.; Leshchenko, D. V.; Zhigulina, V. V.; Miniaev, M. V. Synthetic Melatoninergic Ligands: Achievements and Prospects. *ISRN Biochem.* **2014**, *2014*, 1–11. https://doi.org/10.1155/2014/843478.

(15) San, L.; Arranz, B. Agomelatine: A Novel Mechanism of Antidepressant Action Involving the Melatonergic and the Serotonergic System. *Eur. Psychiatry* **2008**, *23* (6), 396–402. https://doi.org/10.1016/j.eurpsy.2008.04.002.

(16) Avila, A.; Cardona, X.; Martin-Baranera, M.; Leon, L.; Caballol, N.; Millet, P.; Bello, J. Agomelatine for Depression in Parkinson Disease. *J. Clin. Psychopharmacol.* **2015**, *35* (6), 719–723. https://doi.org/10.1097/JCP.0000000000000404.

(17) Norman, T. R.; Olver, J. S. Agomelatine for Depression: Expanding the Horizons? *Expert Opin. Pharmacother.* **2019**, *20* (6), 647–656. https://doi.org/10.1080/14656566.2019.1574747.

(18) Jockers, R.; Delagrange, P.; Dubocovich, M. L.; Markus, R. P.; Renault, N.; Tosini, G.; Cecon, E.; Zlotos, D. P. Update on Melatonin Receptors: IUPHAR Review 20. *Br. J. Pharmacol.* **2016**, *173* (18), 2702–2725. https://doi.org/10.1111/bph.13536.

(19) P. Zlotos, D. Recent Progress in the Development of Agonists and Antagonists for Melatonin Receptors. *Curr. Med. Chem.* **2012**, *19* (21), 3532–3549. https://doi.org/10.2174/092986712801323153.

(20) Ng, K. Y.; Leong, M. K.; Liang, H.; Paxinos, G. Melatonin Receptors: Distribution in

Mammalian Brain and Their Respective Putative Functions. *Brain Struct. Funct.* **2017**, *222* (7), 2921–2939. https://doi.org/10.1007/s00429-017-1439-6.

(21) Cecon, E.; Oishi, A.; Jockers, R. Melatonin Receptors: Molecular Pharmacology and Signalling in the Context of System Bias. *Br. J. Pharmacol.* **2018**, *175* (16), 3263–3280. https://doi.org/10.1111/bph.13950.

(22) Vakkuri, O.; Leppäluoto, J.; Vuolteenaho, O. Development and Validation of a Melatonin Radioimmunoassay Using Radioiodinated Melatonin as Tracer. *Acta Endocrinol. (Copenh).* **1984**, *106* (2), 152–157. https://doi.org/10.1530/acta.0.1060152.

(23) Dubocovich, M. L.; Takahashi, J. S. Use of 2-[^{125}I]Iodomelatonin to Characterize Melatonin Binding Sites in Chicken Retina. *Proc. Natl. Acad. Sci.* **1987**, *84* (11), 3916–3920. https://doi.org/10.1073/pnas.84.11.3916.

(24) Weaver, D.; Rivkees, S.; Reppert, S. Localization and Characterization of Melatonin Receptors in Rodent Brain by in Vitro Autoradiography. *J. Neurosci.* **1989**, *9* (7), 2581–2590. https://doi.org/10.1523/JNEUROSCI.09-07-02581.1989.

(25) Vaněček, J.; Pavlík, A.; Illnerová, H. Hypothalamic Melatonin Receptor Sites Revealed by Autoradiography. *Brain Res.* **1987**, *435* (1–2), 359–362. https://doi.org/10.1016/0006-8993(87)91625-8.

(26) Vaněček, J. Melatonin Binding Sites. *J. Neurochem.* **1988**, *51* (5), 1436–1440. https://doi.org/10.1111/j.1471-4159.1988.tb01108.x.

(27) Williams, L. M.; Morgan, P. J.; Hastings, M. H.; Lawson, W.; Davidson, G.; Howell, H. E. Melatonin Receptor Sites in the Syrian Hamster Brain and Pituitary. Localization and

Characterization Using [125 |]Lodomelatonin. *J. Neuroendocrinol.* **1989**, *1* (5), 315–320. https://doi.org/10.1111/j.1365-2826.1989.tb00122.x.

(28) Fauteck, J. D.; Lerchl, A.; Bergmann, M.; Møller, M.; Fraschini, F.; Wittkowski, W.; Stankov, B. The Adult Human Cerebellum Is a Target of the Neuroendocrine System Involved in the Circadian Timing. *Neurosci. Lett.* **1994**, *179* (1–2), 60–64. https://doi.org/10.1016/0304-3940(94)90935-0.

(29) Piketty, V.; Pelletier, J. Melatonin Receptors in the Lamb Pars Tuberalis/Median Eminence throughout the Day. *Neuroendocrinology* **1993**, *58* (3), 359–365. https://doi.org/10.1159/000126563.

(30) Adamah-Biassi, E.; Zhang, Y.; Jung, H.; Vissapragada, S.; Miller, R.; Dubocovich, M. Distribution of MT_1 Melatonin Receptor Promoter-Driven RFP Expression in the Brains of BAC C3H/HeN Transgenic Mice. *J. Histochem. Cytochem.* **2014**, *62* (1), 70–84. https://doi.org/10.1369/0022155413507453.

(31) MTNR1B https://www.proteinatlas.org/ENSG00000134640-MTNR1B/tissue.

(32) MTNR1A https://www.proteinatlas.org/ensg00000168412-mtnr1a.

(33) MTNR1B - RP_050331_04_A05 - sagittal https://mouse.brain-map.org/experiment/show/69258178.

(34) Bars, D. L.; Thivolle, P.; Vitte, P. .; Bojkowski, C.; Chazot, G.; Arendt, J.; Frackowiak, R. S. .; Claustrat, B. PET and Plasma Pharmacokinetic Studies after Bolus Intravenous Administration of [^{11}C]Melatonin in Humans. *Int. J. Radiat. Appl. Instrumentation. Part B. Nucl. Med. Biol.* **1991**, *18* (3), 357–362. https://doi.org/10.1016/0883-2897(91)90132-

5.

(35) Chirakal, R.; Sayer, B. G.; Firnau, G.; Garnett, E. S. Synthesis of F-18 Labelled Fluoro-Melatonins and 5-Hydroxy-Fluoro-Tryptophans. *J. Label. Compd. Radiopharm.* **1988**, *25* (1), 63–71. https://doi.org/10.1002/jlcr.2580250108.

(36) Chen, J. J.; Fiehn-Schulze, B.; Brough, P. A.; Snieckus, V.; Firnau, G. Synthesis of 2-Iodo- and 2-Phenyl-[^{11}C]Melatonin: Potential PET Tracers for Melatonin Binding Sites. *Appl. Radiat. Isot.* **1998**, *49* (12), 1573–1579. https://doi.org/10.1016/S0969-8043(98)00005-0.

(37) Al-Jammaz, I.; Al-Otaibi, B.; Aboul-Enein, H.; Amartey, J. K. Synthesis and Biodistribution of 2-[^{123}I]Iodomelatonin in Normal Mice. *Appl. Radiat. Isot.* **2006**, *64* (1), 38–42. https://doi.org/10.1016/j.apradiso.2005.06.012.

(38) Takashima-Hirano, M.; Tazawa, S.; Takahashi, K.; Doi, H.; Suzuki, M. Efficient Synthesis of [^{11}C]Ramelteon as a Positron Emission Tomography Probe for Imaging Melatonin Receptors Involved in Circadian Rhythms. *Chem. Pharm. Bull.* **2011**, *59* (8), 1062–1064. https://doi.org/10.1248/cpb.59.1062.

(39) Rivara, S.; Lodola, A.; Mor, M.; Bedini, A.; Spadoni, G.; Lucini, V.; Pannacci, M.; Fraschini, F.; Scaglione, F.; Sanchez, R. O.; Gobbi, G.; Tarzia, G. N -(Substituted-Anilinoethyl)Amides: Design, Synthesis, and Pharmacological Characterization of a New Class of Melatonin Receptor Ligands. *J. Med. Chem.* **2007**, *50* (26), 6618–6626. https://doi.org/10.1021/jm700957j.

(40) Ochoa-Sanchez, R.; Comai, S.; Lacoste, B.; Bambico, F. R.; Dominguez-Lopez, S.; Spadoni, G.; Rivara, S.; Bedini, A.; Angeloni, D.; Fraschini, F.; Mor, M.; Tarzia, G.;

Descarries, L.; Gobbi, G. Promotion of Non-Rapid Eye Movement Sleep and Activation of Reticular Thalamic Neurons by a Novel MT_2 Melatonin Receptor Ligand. *J. Neurosci.* **2011**, *31* (50), 18439–18452. https://doi.org/10.1523/JNEUROSCI.2676-11.2011.

(41) Ochoa-Sanchez, R.; Rainer, Q.; Comai, S.; Spadoni, G.; Bedini, A.; Rivara, S.; Fraschini, F.; Mor, M.; Tarzia, G.; Gobbi, G. Anxiolytic Effects of the Melatonin MT_2 Receptor Partial Agonist UCM765: Comparison with Melatonin and Diazepam. *Prog. Neuro-Psychopharmacology Biol. Psychiatry* **2012**, *39* (2), 318–325. https://doi.org/10.1016/j.pnpbp.2012.07.003.

(42) Lopez-Canul, M.; Palazzo, E.; Dominguez-Lopez, S.; Luongo, L.; Lacoste, B.; Comai, S.; Angeloni, D.; Fraschini, F.; Boccella, S.; Spadoni, G.; Bedini, A.; Tarzia, G.; Maione, S.; Granados-Soto, V.; Gobbi, G. Selective Melatonin MT_2 Receptor Ligands Relieve Neuropathic Pain through Modulation of Brainstem Descending Antinociceptive Pathways. *Pain* **2015**, *156* (2), 305–317. https://doi.org/10.1097/01.j.pain.0000460311.71572.5f.

(43) Spadoni, G.; Bedini, A.; Lucarini, S.; Mari, M.; Caignard, D.-H. H.; Boutin, J. A.; Delagrange, P.; Lucini, V.; Scaglione, F.; Lodola, A.; Zanardi, F.; Pala, D.; Mor, M.; Rivara, S. Highly Potent and Selective MT_2 Melatonin Receptor Full Agonists from Conformational Analysis of 1-Benzyl-2-Acylaminomethyl-Tetrahydroquinolines. *J. Med. Chem.* **2015**, *58* (18), 7512–7525. https://doi.org/10.1021/acs.jmedchem.5b01066.

(44) Ettaoussi, M.; Sabaouni, A.; Rami, M.; Boutin, J. A.; Delagrange, P.; Renard, P.; Spedding, M.; Caignard, D.-H.; Berthelot, P.; Yous, S. Design, Synthesis and Pharmacological Evaluation of New Series of Naphthalenic Analogues as Melatoninergic

(MT_1/MT_2) and Serotoninergic 5-HT2C Dual Ligands (I). *Eur. J. Med. Chem.* **2012**, *49*, 310–323. https://doi.org/10.1016/j.ejmech.2012.01.027.

(45) Wager, T. T.; Hou, X.; Verhoest, P. R.; Villalobos, A. Moving beyond Rules: The Development of a Central Nervous System Multiparameter Optimization (CNS MPO) Approach To Enable Alignment of Druglike Properties. *ACS Chem. Neurosci.* **2010**, *1* (6), 435–449. https://doi.org/10.1021/cn100008c.

(46) Wager, T. T.; Hou, X.; Verhoest, P. R.; Villalobos, A. Central Nervous System Multiparameter Optimization Desirability: Application in Drug Discovery. *ACS Chem. Neurosci.* **2016**, *7* (6), 767–775. https://doi.org/10.1021/acschemneuro.6b00029.

(47) Capsoni, S.; Stankov, B. M.; Fraschini, F. Reduction of Regional Cerebral Blood Flow by Melatonin in Young Rats. *Neuroreport* **1995**, *6* (9), 1346–1348. https://doi.org/10.1097/00001756-199506090-00029.

(48) Rivara, S.; Vacondio, F.; Fioni, A.; Silva, C.; Carmi, C.; Mor, M.; Lucini, V.; Pannacci, M.; Caronno, A.; Scaglione, F.; Gobbi, G.; Spadoni, G.; Bedini, A.; Orlando, P.; Lucarini, S.; Tarzia, G. N-(Anilinoethyl)Amides: Design and Synthesis of Metabolically Stable, Selective Melatonin Receptor Ligands. *ChemMedChem* **2009**, *4* (10), 1746–1755. https://doi.org/10.1002/cmdc.200900240.

(49) Morimoto, H.; Fujiwara, R.; Shimizu, Y.; Morisaki, K.; Ohshima, T. Lanthanum(III) Triflate Catalyzed Direct Amidation of Esters. *Org. Lett.* **2014**, *16* (7), 2018–2021. https://doi.org/10.1021/ol500593v.

(50) Yushkevich, P. A.; Piven, J.; Hazlett, H. C.; Smith, R. G.; Ho, S.; Gee, J. C.; Gerig, G. User-Guided 3D Active Contour Segmentation of Anatomical Structures: Significantly

Improved Efficiency and Reliability. *Neuroimage* **2006**, *31* (3), 1116–1128. https://doi.org/10.1016/j.neuroimage.2006.01.015.

(51) Papp, E. A.; Leergaard, T. B.; Calabrese, E.; Johnson, G. A.; Bjaalie, J. G. Waxholm Space Atlas of the Sprague Dawley Rat Brain. *Neuroimage* **2014**, *97*, 374–386. https://doi.org/10.1016/j.neuroimage.2014.04.001.

(52) Seidlitz, J.; Sponheim, C.; Glen, D.; Ye, F. Q.; Saleem, K. S.; Leopold, D. A.; Ungerleider, L.; Messinger, A. A Population MRI Brain Template and Analysis Tools for the Macaque. *Neuroimage* **2018**, *170*, 121–131. https://doi.org/10.1016/j.neuroimage.2017.04.063.